Roll-to-Roll Transfer Printing of Reduced Graphene Oxide Thin Film

by

Hyun-woo Jang

B.Sc., Seoul National University of Science and Technology, 2013

Thesis Submitted in Partial Fulfillment of the
Requirements for the Degree of
Master of Applied Science

in the
School of Mechatronic Systems Engineering
Faculty of Applied Sciences

SIMON FRASER UNIVERSITY

Summer 2015

Approval

Name:	**Hyun-woo Jang**
Degree:	**Master of Applied Science**
Title:	***Roll-to-Roll Transfer Printing of Reduced Graphene Oxide Thin Film***
Examining Committee:	**Chair:** Siamak Arzanpoor Associate Professor

Woo Soo Kim
Senior Supervisor
Assistant Professor

Edward Jung Wook Park
Supervisor
Professor

Flavio Firmani
Internal Examiner
Lecturer

Date Defended/Approved: August 11, 2015

Abstract

A novel thin film transfer mechanism has been studied and developed to transfer chemically reduced graphene oxide (r-GO) thin film using a roll-to-roll printing system. We discover that shear stress generated on the silicon rubber stamp surface facilitates delamination of the deposited r-GO thin film efficiently.

A roll-to-roll apparatus is assembled to demonstrate the shear-induced transfer printing in a large scale printing system. Shear stress is applied on the stamp surface by rotating the stamp side roller faster than the substrate side roller.

The hydrophobic surface is changed to hydrophilic by polydopamine modification for 15 minutes at 60˚C in order for r-GO thin film to be directly deposited on the rubber stamp.

Roll-to-roll printing parameters such as evaporation time during deposition of r-GO, vertical deformation of stamp, RPM, and RPM ratio between two rollers are investigated and adjusted for successful transfer of r-GO.

With the adjusted roll-to-roll printing parameters, r-GO thin film has been transferred successfully to glass and PET substrates at a printing rate of 5mm/min. The shear stress required to transfer r-GO thin film in our experiment condition with glass substrate is estimated to be 325.43 kPa by experimental data and computation with ANSYS.

A flexible transparent capacitive touch sensor is fabricated with printed r-GO thin film after the sheet resistance is significantly improved by thermal annealing process.

Both the shear-induced roll-to-roll printing method and the stamp modification process are expected to contribute to large scale manufacturing systems for flexible printed electronics.

Keywords: Roll-to-roll manufacturing; Transfer printing; Dry transfer; Printed electrode; Reduced graphene oxide; Transparent conductor

To Jesus and my family

Acknowledgements

I truly appreciate Dr. Woo Soo Kim, my senior supervisor, for his continuous and dedicated supervision for my entire school years. He has instructed me patiently though I had made many mistakes. He always keeps my project in his mind and tries to find good information and sources for my project. I thank God for having him as my supervisor. I also would like to thank my defence committee memebers, Dr. Edward Jung Wook Park and Dr. Flavio Firmani, for their willingness to be my supervisor and committee member and their precious time to review my work.

I have been very lucky having good lab mates. I thank Jiseok Kim for his friendly advices on my lab life and research when I was in distress. Rouzbeh has been a good friend of mine helping each other sincerely. Kyle, I could enjoy active life in Vancouver playing with him. Kimball helped me to use 3D printer for roll-to-roll apparatus components and taught how to handle step motor controllers. Abrar, I enjoyed serious talks with him about life and thank him for your kind help whenever I needed. Jason, another Korean guy in our lab, gave me great comfort sharing difficulties and helping each other out.

I would like to express my deepest gratitude to Jesus, my saviour and comforter, and my lovely wife Ara. Everything has made possible by the grace of my God and without God, I would not be able to overcome hardships in my life and research during past years. I thank God for giving me Ara as my wife. She is more than a dream girl I have ever imagined for my wife. I appreciate for her prayer and dedicated support. She always makes delicious foods for me and does houseworks so that I can focus on my thesis project despite she also works full time.

Table of Contents

List of Tables

List of Figures

List of Acronyms

3D	Three Dimension
AFM	Atomic Force Microscopy
ATR-IR	Attenuated Total Reflextance Infrared Spectroscopy
CVD	Chemical Vapor Deposition
DI water	Distilled water
DMF	Dimethyl Formamide
EC	Ethyl Cellulose
GO	Graphene Oxide
HOPG	Highly Ordered Pyrolytic Graphite
ITO	Indium Tin Oxide
LED	Light Emitting Diode
OLED	Organic Light Emitting Diode
PDMS	Polydimethylsiloxane
PET	Polyethylene Terephthalate
PLA	Poly Lactic Acid
PMMA	Poly Methyl MethAcrylate
RPM	Revolutions Per Minute
r-GO	Reduced graphene Oxide
SEM	Scanning Electron Microscope
UV	Ultraviolet
UV-Vis	Ultraviolet-Visible Spectroscopy

Chapter 1.

Introduction

1.1. Motivation

The demand of wearable and flexible devices such as flexible sensors for health monitoring [1], flexible displays [2], and stretchable energy storage [3] has been significantly increased. The flexible sensor technology is moving closely related with the development of stretchable and flexible electrodes. Not only is the development of electrode materials important, but also deposition techniques, patterning processes, and combining them into a manufacturing system are significant, thus having been spotlighted by relevant scientists and engineers.

Graphene has been highlighted as a promising advanced material for its electrical and mechanical properties since Andre Geim and his co-workers at the University of Manchester introduced a simple way to produce graphene sheets [4], [5]. The requirements to be a flexible electrode are satisfied by properties of graphene. Though it is expected by many people that graphene will be a dominating conductive material for flexible electrodes in the near future, its large scale production method and the appropriate film transfer technology for the mass production of devices still remain as unsolved assignments.

1.2. Objective

The objectives of this thesis are summarized as below

- Large scale manufacturing of flexible application of reduced graphene oxide (r-GO) thin film using compliant rubber stamps.

- Roll-to-roll printing of r-GO using a novel mechanism, named shear-induced transfer, which is purely contributed by mechanical shear stress.
- Design and fabrication of a roll-to-roll apparatus that can facilitate shear-induced transfer.
- Optimization of parameters in roll-to-roll shear-induced transfer printing.
- Optimization of electrical property of the transferred r-GO thin film.

1.3. Contribution

This thesis mainly contributed to four areas: 1. r-GO thin film deposition method on hydrophobic stamp surface. 2. Development of a new film transfer mechanism named shear-Induced transfer in which shear stress is the main source of the mechanism. 3. Design and fabrication of a roll-to-roll apparatus that can utilize shear-induced transfer printing mechanism. 4. Optimization of electrical property of transferred r-GO thin film.

In organic device fabrication, the selection of film deposition technologies has to be carefully considered depending on the property of the material and the substrate. For example, the direct deposition of solution-processed materials like chemically reduced GO by a variety of methods such as inkjet printing, screen printing, dropcasting, spray, etc. can sometimes degrade or change the substrate material chemically because of the existence of organic solvents, thus making its deposition and patterning process difficult and limited. Therefore, dry transfer (or transfer printing) using patterned stamps is a good way to pattern and deposit a film when chemical damages and degradation on the substrate are issues.

There are two big assignments for transfer printing to be successfully done especially when using rubber stamp and solution processed r-GO: 1.Depositing r-GO thin film on the stamp is difficult because silicon rubber surface is too hydrophobic to form a uniform film by dropcasting. 2.Transfer of r-GO thin films to the substrate in a short time without adhesive has not been introduced yet.

This thesis provides solutions for those assignments stated in the previous paragraph. Stamp surface modification technology has been developed as well as the process optimization which enabled the direct deposition of solution-processed

chemically reduced graphene oxide thin film on the stamp surface by dropcasting. Also, a new film transfer mechanism, named shear-induced transfer, for r-GO thin film has been developed. Our shear-induced transfer does not require the use of heat and chemicals, let alone adhesive. Furthermore, this transfer mechanism is demonstrated in a Roll-to-Roll printing system designed for shear-induced transfer, opening the doors towards large scale manufacturing systems for printed flexible electronics. A post-treatment process (thermal annealing) which is investigated to improve electrical property of transferred r-GO thin film ends up with removal of residues on r-GO thin film, therefore dramatically reducing sheet resistance. Transfer parameter optimization and film characterization are also significant parts of this thesis that contributes to r-GO transfer technology.

1.4. Thesis Organization

The organization of this thesis is as follows. In the rest of chapter 1, background of graphene is introduced, giving basic idea about properties of graphene, preparation methods, how graphene is patterned and deposited, and its applications. Chapter 2 starts with introducing roll-to-roll printing systems applied to printed electronics manufacturing systems and describes the design, specification and control method of our roll-to-roll apparatus for shear-induced transfer. Chapter 3 presents a whole picture of shear-induced transfer of r-GO with experimental data and discussions on the mechanisms. Stamp surface modification method for dropcasting of r-GO followed by r-GO preparation section, the optimization process of the transferred r-GO, and demonstration of the transferred thin film are described here. Finally, conclusion and future work to do are discussed in the last chapter.

1.5. Introduction of Graphene

1.5.1. Opportunity with Graphene

Development of transparent electrode materials that can work at certain strain levels has become a common goal of researchers. As the world has been experiencing a rapid change by development of ubiquitous and environment-friendly portable devices, it is expected that electronics industry will be focusing more on devices that are flexible, wearable, and stretchable. In this era, conventional materials like silicon, semiconducting material, and Indium tin oxide (ITO), transparent electrode, need to be replaced because those are not flexible.

It has been agreed by many researchers that graphene is a promising material that is enough to replace silicon and ITO [6], [7]. Graphene is a 2-dimensional carbon material which is flexible, stretchable, transparent and conductive. The advent of graphene by Andre Geim et al.[4] in 2004 (they discovered a very simple method, called Scotch tape method, to produce graphene, and they characterized properties of graphene) aroused strong interest of people from material science and many applied science areas who were keen to find materials that can replace silicon and ITO. The significance of this material is proved by 2010 Nobel Prize in physics. Thousands of papers about graphene and the applications have been published so far making steps forward to industry level facilitation of graphene materials.

1.5.2. Structure of Graphene

Graphene is a two-dimensional layer of sp^2-bonded carbon atoms with the hexagonal lattice structure. The graphene hexagonal lattice is composed of two sub-lattices of carbon atoms bonded together with σ bonds [8]. The thickness of single layer graphene has been known to be less than 0.35 nm and the distance between carbon atoms is 0.142nm. Graphene is also known as a single layer of graphite and Andre Geim et al.[4] first succeeded in separating single layer of graphite by mechanical exfoliation Figure 1.1).

In reality, graphene film does not always have the perfect two-dimensional honeycomb structure over the whole film area. A. Fasolino et al.[8] found that a graphene film is not perfectly flat but has ripples (Figure 1.2). They discovered that the ripples on the surface are because of thermal fluctuations and this is due to the multiplicity of chemical bonding in carbon. Kwangpyo Kim et al. [9] also reported that graphene films grown on copper foil by a Chemical Vapor Deposition (CVD) process have not only the honeycomb lattices but also pentagonal and heptangular lattices (Figure 1.3). It is also observed that direction of the crystal structure is not always uniform and there are non-hexagonal lattices along the border between two different grains (Figure 1.3).

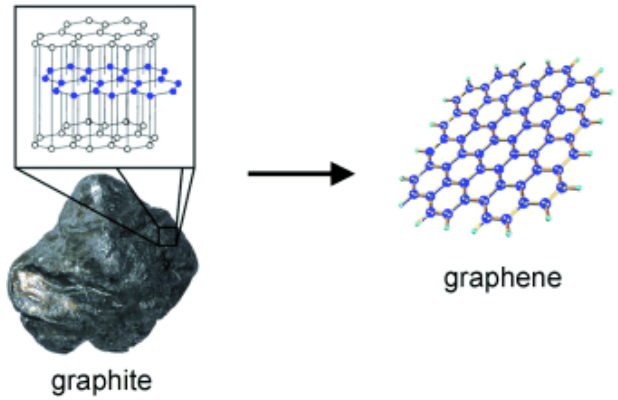

Figure 1.1. Schematic explanation of graphene structure [10]. Reprinted with permission.

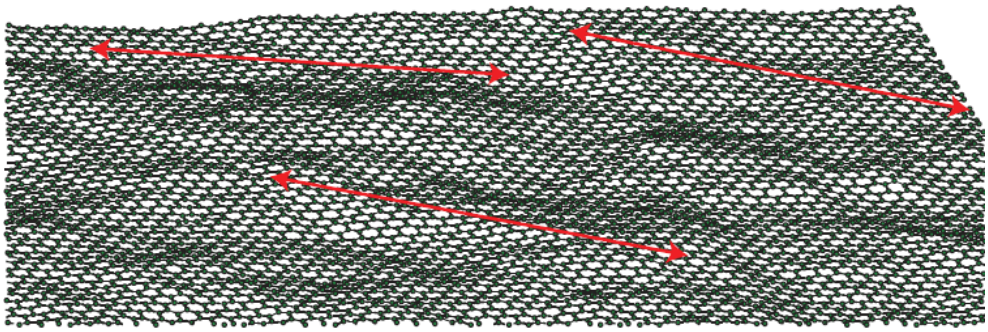

Figure 1.2. Simulated graphene film surface feature with ripples [8]. Reprinted with permission.

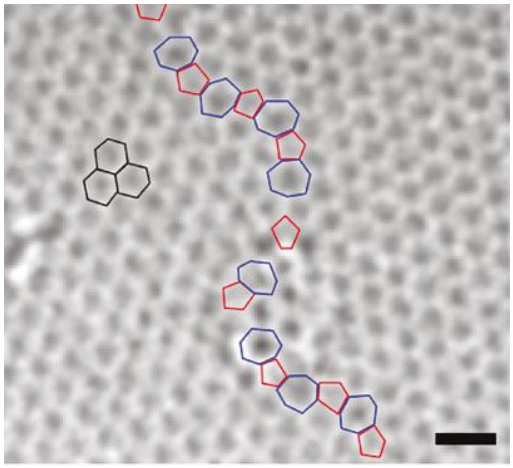

Figure 1.3. **Atomic-resolution image of a graphene. The pentagon, hexagon, and heptagon are colored with red, black, and blue polygons, respectively. The scale bar is 0.5nm [9]. Reprinted with permission.**

1.6. Preparation and Patterning of Graphene Thin Film

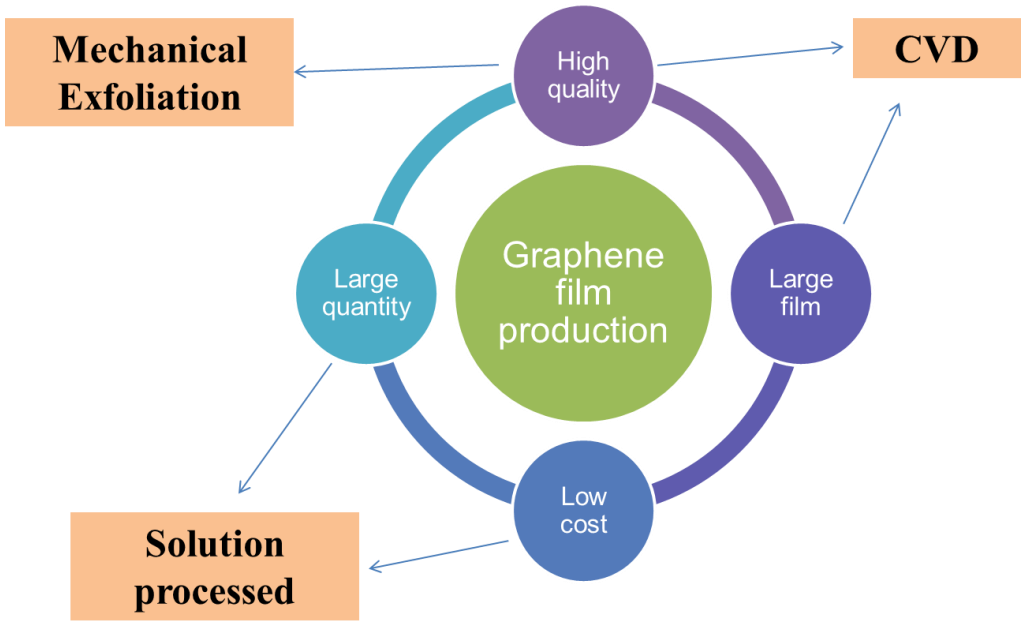

Figure 1.4. **Diagram of the characteristics of graphene film production methods.**

Electrical conductivity, film size, production cost, production scale, deposition method, and patterning method become significantly different depending on the graphene synthesis method. As described in Figure 1.4, high quality (in conductivity) graphene films are generally generated by either mechanical exfoliation method or CVD, while those two are relatively expensive and not yet developed well for mass production as much as solution processed graphene. Solution processed graphene materials are good candidates for cheap and a large scale synthesis though its electrical properties are the least among those three. The CVD method can synthesize one big single layered graphene sheet, whereas graphene films prepared by other methods usually consist of small graphene flakes [11]. Deposition and patterning methods also varies among them. This will be discussed in following section with examples.

1.6.1. Mechanical Exfoliation

Mechanical exfoliation is a method that cleaves graphite layers into single or few layers by mechanical force. Graphene is a single layer of graphite. While carbon atoms have covalent bonding in the lateral direction, the vertical direction interaction between graphene sheets is van der Waals interaction which is much weaker than covalent bonding. In addition, the friction between layers is low so that exfoliation of a graphene layer can be accomplished with little pulling or sliding force [12]. Since this method produces high quality graphene sheets with almost no defect and impurity, the resulting graphene is a good source for academic researches. However, its yield and throughput are extremely low and the flake size is micro-scale, limiting its application.

By Dongsheng Li et al.[13] demonstrated the production of a pattern of mechanically exfoliated graphene sheets. They made an array of squares on highly ordered pyrolytic graphite (HOPG) by photolithography to use it as a patterned stamp as described in Figure 1.5(a) and the resulting images of the stamp by Scanning Electron Microscope (SEM) are shown in Figure 1.5(b). To exfoliate the single or few layers of graphene on the stamp, pulling force has to be exerted on the stamp surface in any way. They used van der Waals force difference that a graphene layer has with another layer

of graphene and the substrate (SiO_2) to transfer graphene film onto the substrate. The cohesion energy of SiO_2 is around 8.6 times higher than that of graphite and this big interaction energy difference ensures the transfer of graphene layers to the substrate. Thus, the stamping process is simple as shown in Figure 1.6. The stamping result is displayed in Figure 1.7. Graphene sheets were printed on the substrate keeping the stamp pattern (Figure 1.7(a)). The colors of printed graphene were differently taken by optical microscope due to the height difference. The heights of squares of each color were measured by Atomic force microscopy (AFM) scanning and presented in (Figure 1.7(c)). Majority of printed squares are too thick to be called few layered graphene. Their approach successfully demonstrated the patterning of high quality mechanically exfoliated graphene layers, but they could not reach to getting high yield of single or few layer graphene, which is a fundamental drawback of mechanical exfoliation method.

Patterning of mechanically exfoliated graphene has been explored by many researchers and many of them used HOPG and stamping methods [14]. Though people produced patterns of high quality graphene layers with precise pattern positioning technology, they could not control the number of graphene layers. Also, the stamping process required vacuum condition or adhesive to control the adhesion. For these reasons, mechanically exfoliated graphene has been limited its usage to fundamental studies.

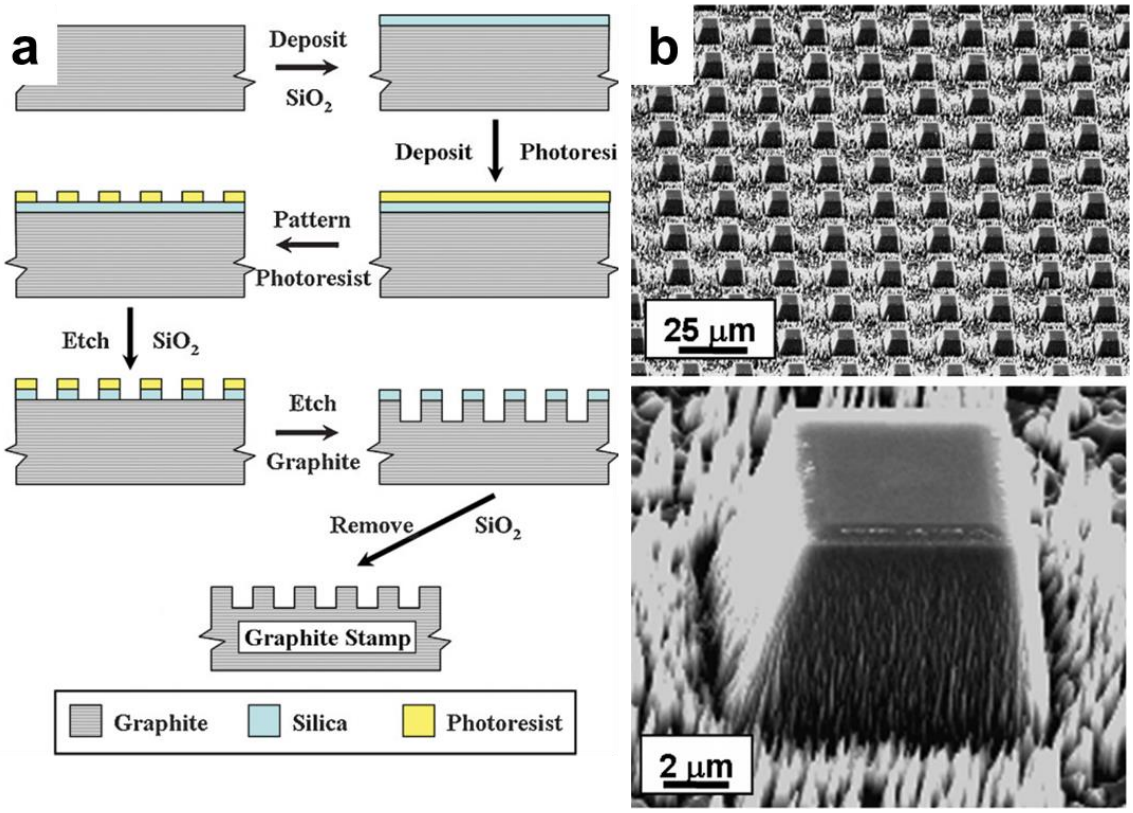

Figure 1.5. **(a) Graphite stamp fabrication flow. (b) SEM images of the graphite stamp [13]. Reprinted with permission.**

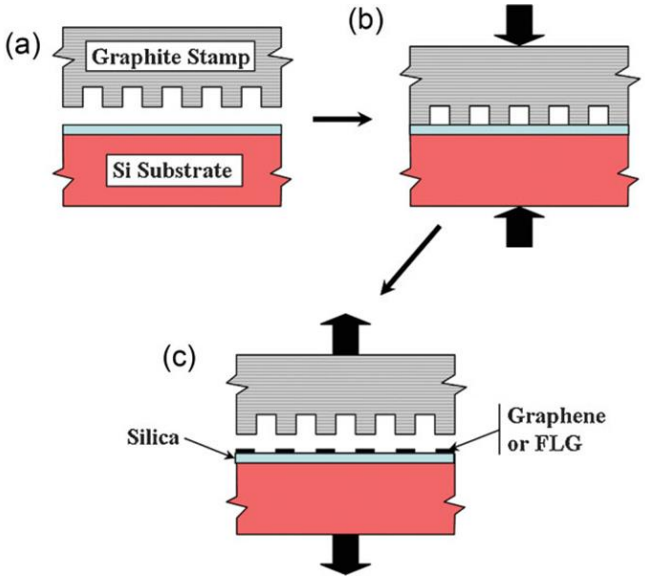

Figure 1.6. **Schematic illustration of the stamping process [13]. Reprinted with permission.**

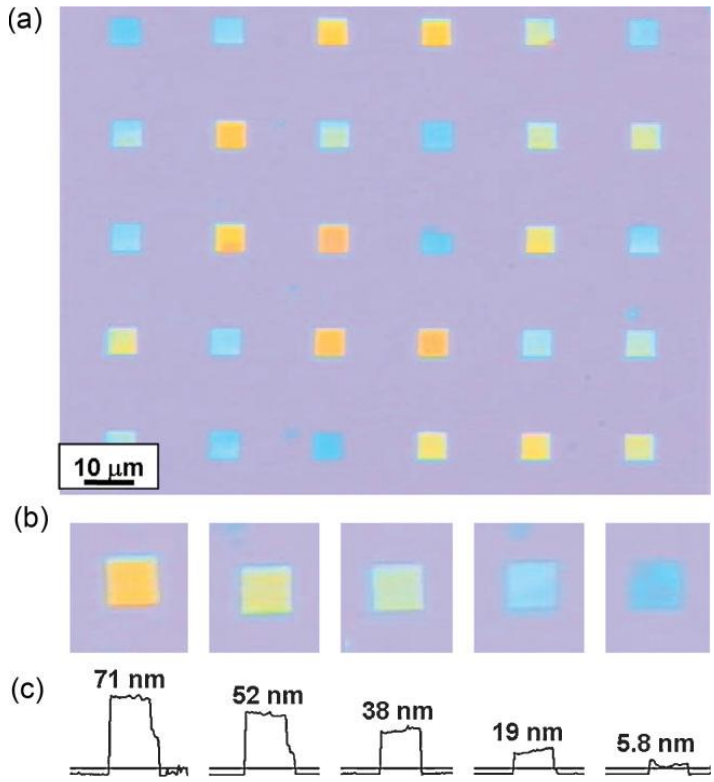

Figure 1.7. Optical images of (a) transferred graphene pattern. The color difference is due to different heights: (b) stamped individual squares with different height, (c) AFM scanning profiles and measured heights of stamped squares in (b) [13]. Reprinted with permission.

1.6.2. Chemical Vapour Deposition

Chemical vapour deposition (CVD) enables large film size of high quality single or few layered graphene films. It is cheaper method and has relatively larger throughput than mechanical exfoliation though the solution processed graphene stand out from them with respect to cost and production scale [7][11].

CVD synthesizes a graphene film on transition metals such as nickel and copper that can absorb carbon atoms well [15]. The catalyst metal foil is placed in the CVD chamber and methane (CH_4) and hydrogen (H_2) gases are introduced in the chamber. As the temperature inside of the chamber increases up to around 500~1000˚C [16][17], carbon atoms are dissolved into the metal substrate. After proper amount of carbon is absorbed in the metal foil, temperature is brought down to room temperature and vacuum is drawn to remove exhaust gaseous species after completion of reactions. As

temperature decreases, the solubility of carbon atom in the metal decreases and the metal starts to diffuse carbon atoms onto the surface forming a graphene layer. The cooling rate is a parameter to determine the thickness of graphene thin film. The thickness of CVD grown graphene can be controlled by adjusting the cooling speed [18]. The graphene film grow process is visualized in Figure 1.8. The metal catalyst is etched away in an etchant bath to transfer the graphene film to a targeted substrate.

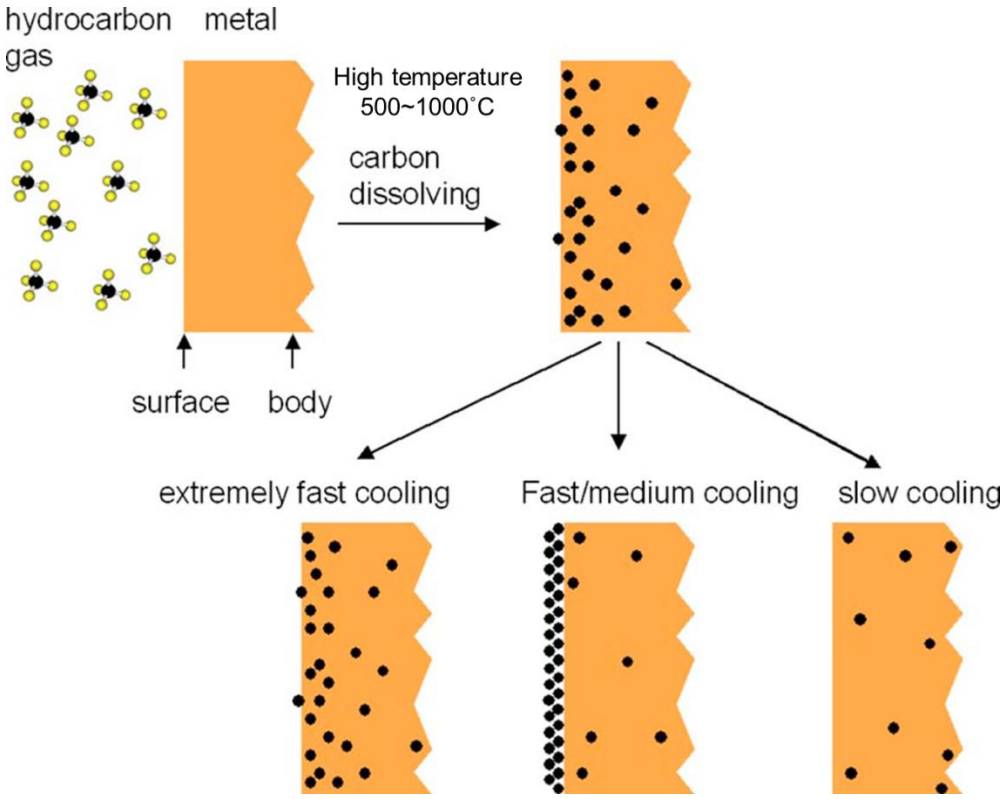

Figure 1.8. Schematic description of graphene film growth in CVD [18]. Reprinted with permission.

For transfer of CVD grown graphene, Sukang bae et al.[19] successfully demonstrated roll-to-roll transfer of a large area highly conductive and transparent graphene film. They grew a graphene film on a copper foil in a tubular quartz tube at high temperature and attached the graphene/copper film to a thermal release tape. The copper foil was etched away in a roll-to-roll section with an etchant bath. The graphene film on the thermal release tape is ready to be transferred to any substrate with applied heat (90~120˚C) at a transfer rate of 150~200mm/min in the roll-to-roll system. They obtained a graphene film of 97.4% (at 550nm wavelength) transmittance and ~125Ω/□

sheet resistance from their process. They further improved the sheet resistance down to ~30Ω/□ by stacking 4 layers of graphene and doping with HNO_3.

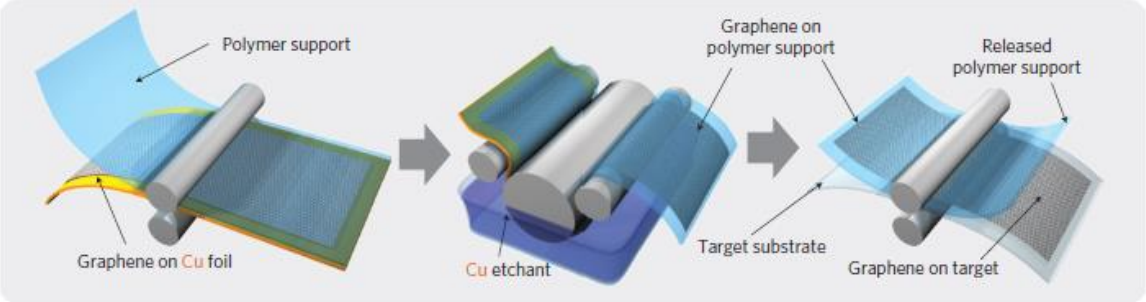

Figure 1.9. Schematic illustration of the roll-to-roll graphene film transfer using a thermal release tape [19]. Reprinted with permission.

Toshiyuki Kobayashi et al.[20] also introduced a roll-to-roll system that synthesize and transfer a large scale (100m long) graphene film continuously at low pressure condition. The development of large scale CVD grown graphene systems introduced above is leading to application of graphene in a broad area though the use of expensive metal catalysts is one another drawback of CVD method.

As for patterning of CVD grown graphene, Keun Soo Kim et al.[15] pre-patterned the Ni catalyst layer to form a graphene layer according to the pattern (Figure 1.10(a)). After the completion of graphene growth on the patterned catalyst foil, they used two different methods to transfer the film onto target substrates. The first method uses a polydimethylsiloxane (PDMS) carrier (Figure 1.10(b)). A PDMS carrier is put on the graphene film and the catalyst layer is etched away leaving the graphene on the PDMS carrier. After the film is dried, the graphene is transferred on to a SiO_2 substrate by a simple stamping process. This method is useful in that it is dry transfer without chemicals. In the other transfer method, graphene on the catalyst film is put into an etchant. As the metal layer is etched away, graphene thin film floats on the etchant surface. The floating graphene thin film is taken onto a substrate by placing the substrate on the graphene thin film (Figure 1.10(c)). The sheet resistance and transparency of the transferred film are ~280Ω/□ and ~80% (at 550nm wavelength) respectively.

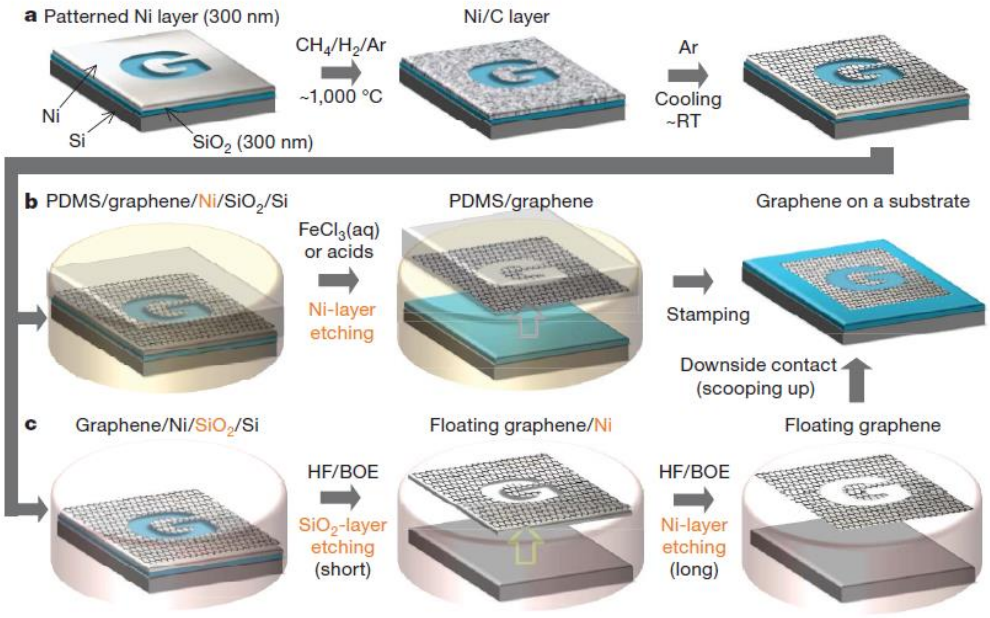

Figure 1.10. Synthesis, etching and transfer of patterned graphene films. (a) Graphene growth on pre-patterned Ni catalyst layer, (b) dry transfer of graphene using a PDMS carrier, (c) transfer of graphene by floating graphene [15]. Reprinted with permission.

Another patterning method was introduced by Seok Ju Kang et al.[21]. They grow a single layer graphene on a copper foil. A micro-scale patterned PDMS stamp is prepared and put on the graphene film. The copper foil is removed by etching. Graphene films remain only on the PDMS stamp posts. After rinsing with Distilled water (DI water), the PDMS stamp inked with graphene films is pressed onto the substrate and then the PDMS stamp is removed (Figure 1.11). They were able to print ~10μm scale 0.7nm thick patterns of sheet resistance of ~1.8kΩ/□.

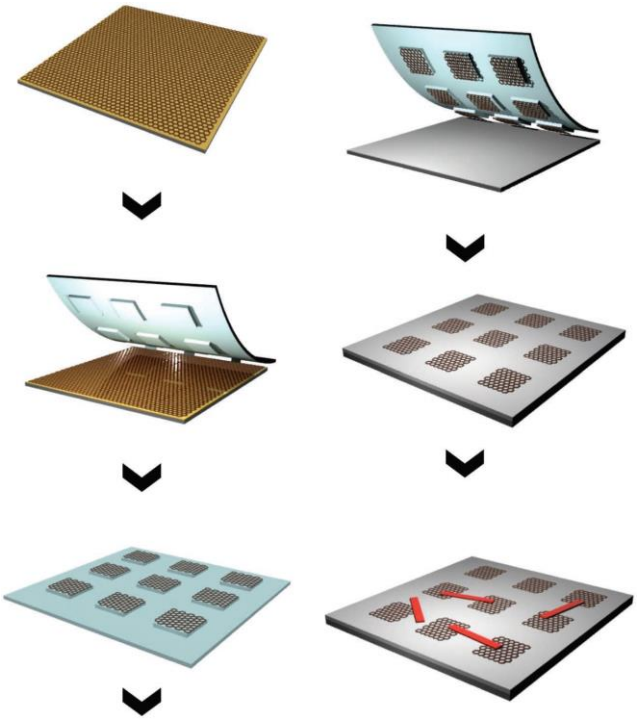

Figure 1.11. Schematic illustration of the graphene film patterning and transfer process developed by Seok Ju Kang et al.[21]. Reprinted with permission.

1.6.3. Solution Processed Graphene

The ability to produce graphene thin films in large scale at low cost is a big advantage of solution processed graphene. It enables large scale graphene thin film formation on flexible substrates and also compatible with various printing technologies. Solution processed graphene is derived from graphite usually by chemical exfoliation in solution, and the graphene sheets stay in solvents stably [22]. For its various film formation and printing methods, there are countless applications especially in printed electronics. Solution processed graphene, however, has a big disadvantage. Electrical conductivity and carrier mobilities of solution processed graphene have been known to be orders of magnitude poorer than that of mechanically exfoliated graphene and CVD grown graphene because of high defect density on the graphene flakes. To further broaden its applicable area, there have been many researches to enhance electrical properties of solution processed graphene[23][24][25].

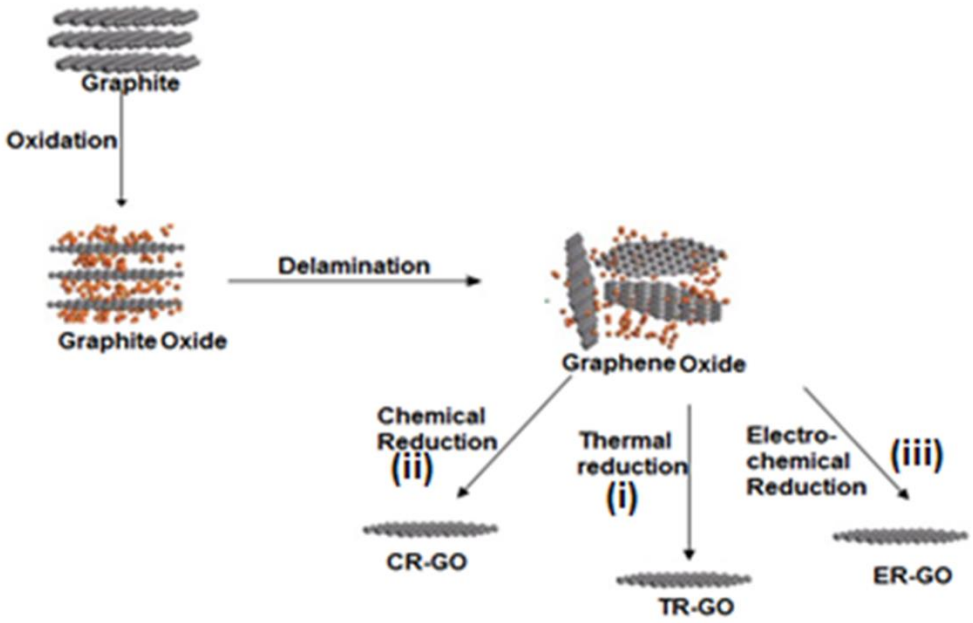

Figure 1.12. Schematic illustration of the production of reduced graphene oxide from graphite [26]. Reprinted with permission.

Solution processed graphene synthesis consists of three big steps (Figure 1.12): 1. Oxidation of graphite, 2. Delamination of graphite oxide into graphene oxide(GO), 3. Reduction of graphene oxide [26].

Step 1 and 2 are mostly done by Hummers' method [27]. Graphite is treated with strong acids such as sulfuric acid (H_2SO_4) and nitric acid (HNO_3) to decorate graphite layers with oxygen containing groups. The oxidized graphite can be exfoliated in water under ultrasonication because the oxygen groups expand the gap between layers and make the layers hydrophilic allowing water molecules to easily intercalate between layers. The exfoliated graphite oxide layers are called graphene oxide (GO). GO loses the characteristics of graphene because there are hydroxyl groups and epoxy groups on the basal plane and carboxylic groups on the edges breaking the sp^2 network of graphene. The oxygen groups have to be removed in order to restore the sp^2 network of graphene.

There are three different methods to reduce graphene oxide (Figure 1.12): 1. Chemical reduction, 2. Thermal reduction, 3. Electrochemical reduction.

To chemically reduce GO, strong reduction agents such as hydrazine (N_2H_4) [28], hydroquinone ($C_6H_6O_2$)[29], hydrogen sulphide (H_2S) [30], and sodium borohydride ($NaBH_4$)[31] are used in solution. There are remaining oxygen groups even after chemical reduction in reality and those can further removed by thermal annealing.

High temperature can facilitate the thermal deoxygenation of GO. When the thermal energy reaches the binding energy between the oxygen groups and graphene, the oxygen groups can be dissociated. Therefore, the restoration of graphene's electrical characteristics depends on the temperature used for reduction. Figure 1.13 shows the relation between conductivity of the thermally reduced graphene oxide sheets and the annealing temperature. Thermal reduction process is usually done after GO is deposited on a substrate and this is one advantage of this method because hydrophilic GO sheets are easier to be stored in solution and deposited on substrates.

Electrochemical reduction of GO is carried out in a normal electrochemical cell using an aqueous buffer solution at room temperature. The main source of reduction is the electron exchange between GO and electrodes, thus not using harmful chemicals like hydrazine [25][32].

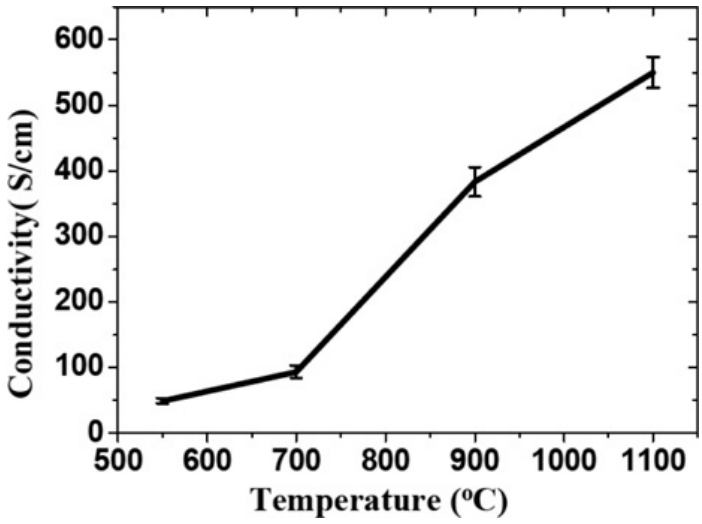

Figure 1.13. Conductivity of thermally reduced graphene oxide sheets according to the temperature [33]. Reprinted with permission.

There are various patterning methods for solution processed graphene. Since graphene sheets are stored in solution, conventional printing technologies such as

gravure[34], flexography[35], inkjet[36], and screen printing[37] are available for solution processed graphene as an ink.

To apply graphene to those listed printing method, formulation of the ink with graphene has to be optimized depending on the required viscosity of the printing method. To increase viscosity and stabilize the graphene ink, polymer binder (ethyl cellulose (EC) is commonly used) in organic solvent is mixed with graphene sheets [34][35][37].

Ethan B. Secor et al.[34] formulated a graphene ink for gravure printing and demonstrated printing of patterned graphene films by gravure printing. Figure 1.14(a) is a schematic of the ink structure formulated with EC in toluene and ethanol solvent. Figure 1.14(b) is the prepared ink ready for printing. They used a conventional gravure printing apparatus and optimized the parameters such as spacing between cells, cavity size, temperature, and printing speed for the graphene ink. The gravure printing process is illustrated in Figure 1.14(c-e). Figure 1.15(a) shows the image of printing graphene lines and they also tried printing the second layer on the first printed layer as shown in Figure 1.15(b). They printed graphene lines of 30μm width and 15~30μm thickness on a rough substrate (Kapton, ~50μm), and the conductivity is ~10,000S/m. There was no conductivity loss even over 500 bending cycles at a radius of 2mm.

For applications in which wet transfer cannot be used, conventional printing methods that use ink are not the option. For those cases, transfer printing of r-GO can be a possible way to pattern and print r-GO thin films. An example of transfer printing is presented in Chapter 3 and also our shear-induced transfer method is a good option.

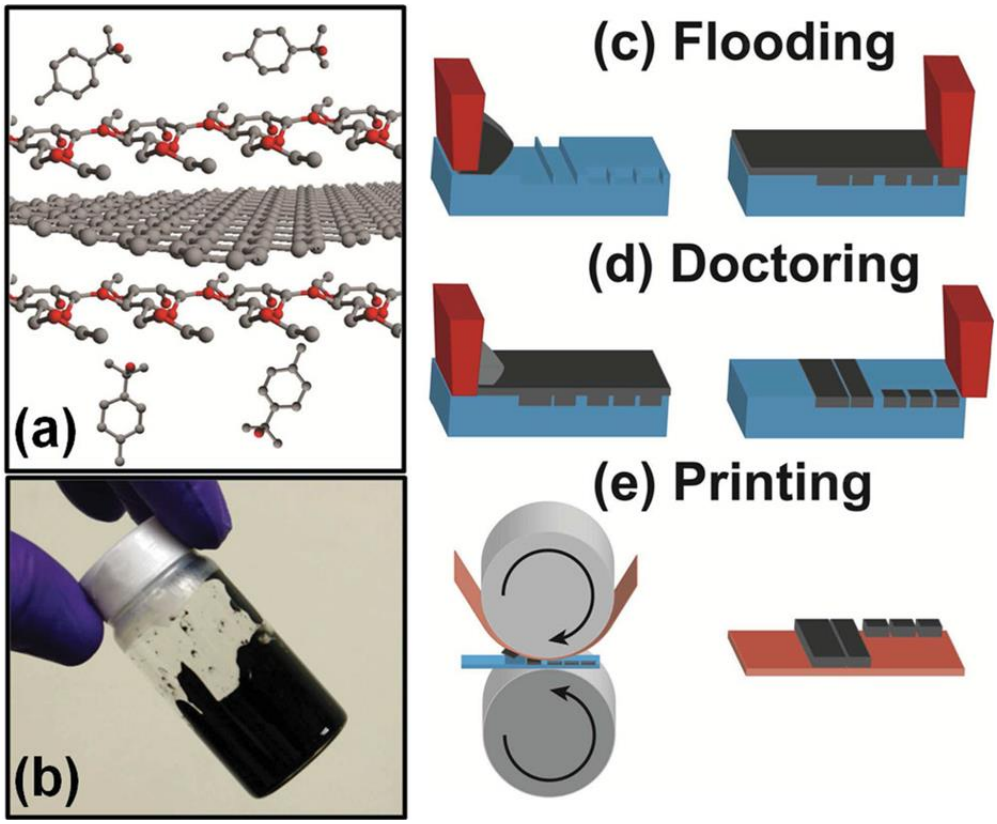

Figure 1.14. **Development of graphene ink and the gravure printing process. (a) schematic of the ink structure with stabilizers. (b) a picture of prepared ink. (c-e) gravure printing process: (c) flooding of the gravure cells, (d) removal of excessive ink by doctor blading, (e) printing onto a flexible substrate [34]. Reprinted with permission.**

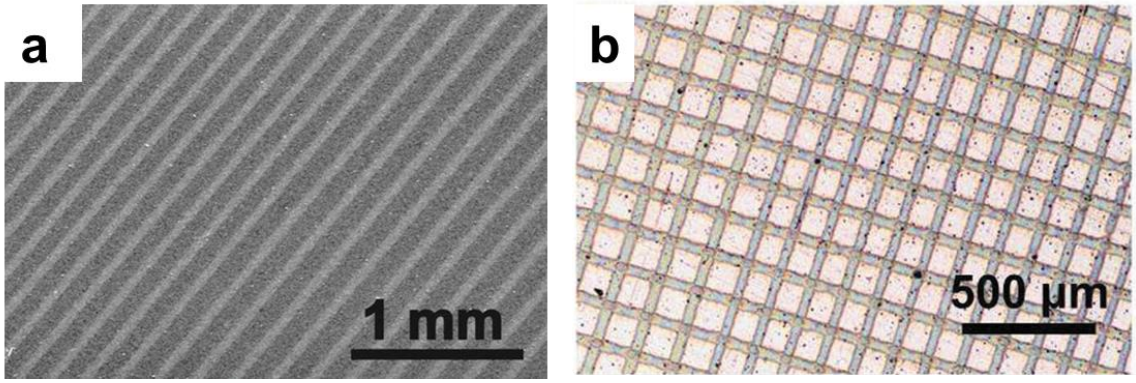

Figure 1.15. **(a) Large-area scanning electron micrograph of printed lines. (b) graphene grid array by printing twice [34]. Reprinted with permission.**

1.7. Applications of Graphene Thin Film

1.7.1. Flexible Transparent Electrode

Development of flexible transparent electrode is an essential step toward commercialization of flexible touch screen, display, organic light emitting diode (OLED), flexible solar cells, and so on. Indium tin oxide (ITO) has been conventionally used for a transparent electrode material. However, ITO is an expensive material and the manufacturing cost is also expensive. In addition, its brittle material property has been hindering its use in flexible devices.

Graphene is a promising alternative for ITO for graphene has superior material properties to ITO. CVD method can synthesize a single or few layered graphene film which is extremely thin and has high optical transmittance. Electrical properties of graphene film are also compatible with ITO. One great advantage of graphene over ITO is that graphene film's electrical property does not change at high strain.

Sukang bae et al.[19] fabricated a touch screen panel with their graphene preparation and transfer method already mentioned above. Their four-layered CVD grown graphene has ~30Ω/□ of sheet resistance and ~90% of optical transmittance which are better than what ITO has. The touch panel can operate at strain level of 6% without performance changes, while commercialized ITO based panel breaks under 2~3% strain. The limited performance after 6% strain is not because of the graphene film but because of the silver electrodes printed on the graphene film.

Zongyou Yin et al.[38] utilized solution processed graphene film as a flexible transparent electrode in an organic solar cell. GO is spin-coated on a clean SiO_2/Si substrate to form a thin film of GO. Subsequently, thermal annealing in Ar/H_2 atmosphere at 1000˚C for 2 hours is applied to reduce the GO film. Prepared r-GO on the SiO_2/Si substrate is transferred onto an oxygen plasma treated PET substrate using polymethyl methacrylate (PMMA) carrier (PMMA is etched with acetone after transfer). Other layers are deposited on the prepared r-GO/PET by spin coating and thermal evaporation (for silver electrodes). The layer structure of the organic solar cell and the energy level diagram are depicted in Figure 1.17 (a) and (b) respectively. r-GO

electrodes of different thicknesses were used to fabricate solar cells and the performances were observed (Table 1.1). The tensile strain of 2.9% was applied on the organic solar cells and they could operate even after a thousand of bending. Though the power conversion efficiency (η%) of their devices is low compared to that of ITO based solar cells, this paves a way to develop printed flexible organic solar cells.

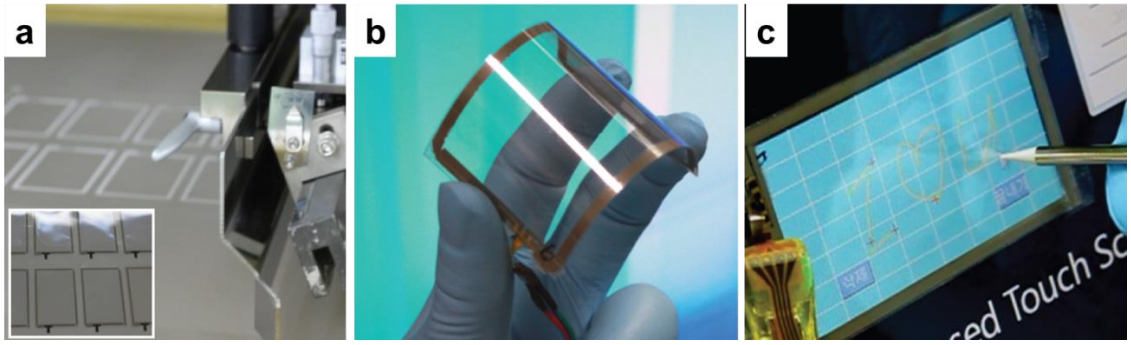

Figure 1.16. **(a) Screen printing of silver past electrodes on graphene flexible electode. (b) demonstration of the flexibility of the graphene based touch panel. (c) demonstration of touch panel conntected to a computer [19]. Reprinted with permission.**

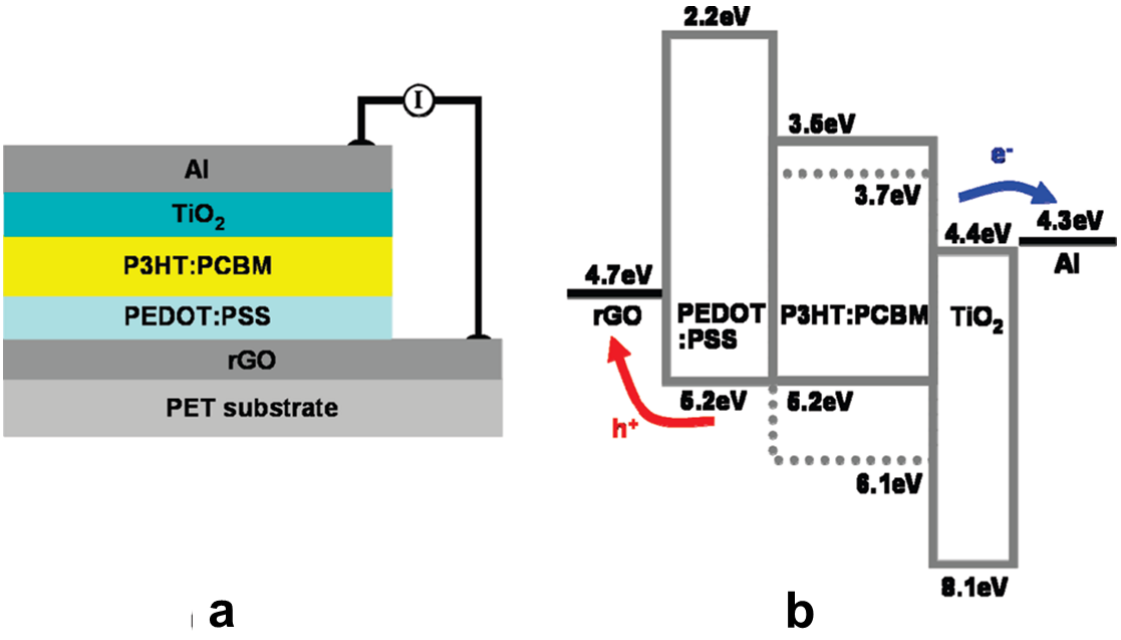

Figure 1.17. **(a) Schematic description of the solar cell layer structure. (b) energy level diagram of the solar cell with r-GO thin film as the transparent electrode [38]. Reprinted with permission.**

Table 1.1. Performance of the flexible organic solar cells with r-GO electrodes of different thicknesses(d), sheet resistance(R), and transmittance(T) [38].

r-GO thin film(d, R, T)	J_{sc} (mA/cm2)	V_{oc} (V)	FF	η(%)
(4nm, 16.0 kΩ/□, 88%)	1.74	0.557	0.30	0.28
(10nm, 6.6 kΩ/□, 78%)	3.31	0.560	0.31	0.61
(16nm, 3.2 kΩ/□, 65%)	4.39	0.561	0.32	0.78
(21nm, 1.6 kΩ/□, 55%)	4.24	0.557	0.32	0.77

1.7.2. Sensor

Graphene also has special characteristics to be utilized as a sensor material. Konstantin S. Novoselov's group at Manchester University developed chemical sensors with mechanically exfoliated graphene knowing that chemical gas molecules absorbed on graphene sheets act as donors or acceptors, changing conductivity of the entire graphene thin film [39]. They succeeded to measure amount of chemicals such as NO_2, NH_3, H_2O, CO, and C_2H_5OH with their graphene based sensors and found that NO_2 and H_2O become electron acceptors and the others become donors. A number of groups have demonstrated good sensitivity of chemically derived graphene for NO_2, NH_3, and dinitrotoluene under ambient conditions [40][41].

Pristine graphene and chemically derived graphene show different responses to chemical gas reaction on sheets. Gas molecules as acceptors or donors increase electron or hole population in pristine graphene and both increase conductivity. On the other hand, since chemically derived graphene is nominally p-type, electron withdrawing groups and electron donators have different responses. Electron withdrawing groups add more on carriers, while electron donators decrease holes [42].

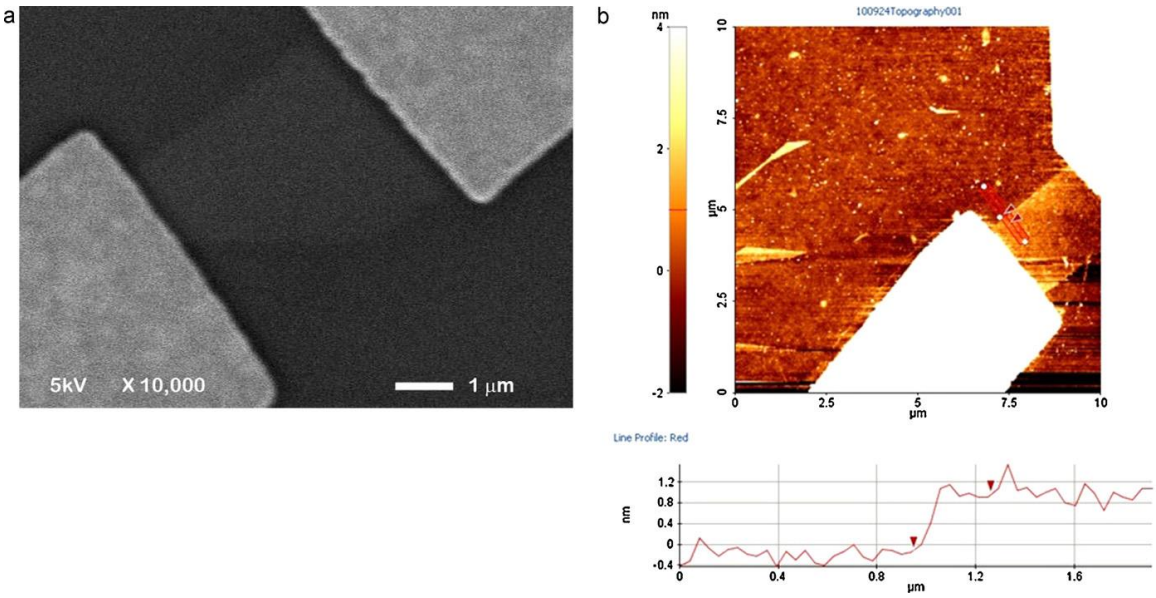

Figure 1.18. (a) SEM image of the fabricated sensor. (b) AFM image of graphene and the electrode, and the graphene thickness measurement profile (bottom) [43]. Reprinted with permission.

Hyeun Joong Yoon et al.[43] demonstrated carbon dioxide sensor using a graphene sheet. They exfoliated few-layered pristine graphene from HOPG and transferred it onto oxidized silicon wafer surface using PDMS stamp. They chose gold for electodes' material and deposited electrodes by standard electron-beam evaporation. Figure 1.18 shows the sensor structure and the thickness of graphene film used as a sensor material. It was observed that the conductance of the graphene gas sensor linearly changes according to the concentration of CO_2 gas in 10~100 ppm range.

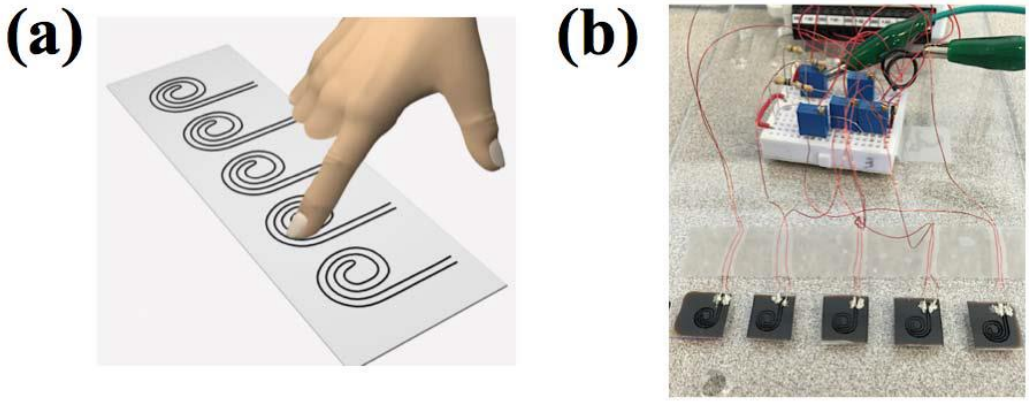

Figure 1.19. (a) Schematic illustration of r-GO pressure sensor. (b) actual image of the sensor interfaces and the circuit [44]. © [2015] IEEE

Rouzbeh Kazemzadeh et al.[44] reported a highly sensitive pressure sensor using photothermally reduced graphene oxide. They deposited GO film on a flexible substrate by dropcasting method and reduced the film using laser beam. The thermal energy obtained from the laser dissociated oxygen containing functional groups on GO film reducing sheet resistance down to 100~500 Ω/□. GO was selectively reduced according to the touch sensor interface pattern as shown in Figure 1.19(a). When pressure is applied on the touch panel, the contact area between r-GO sheets increases leading to lower resistance and the voltage change by resistance variation is recorded to measure the pressure. Their sensor is capable of sensing pressure at a sensitivity of 19 mV/kPa.

Chapter 2.

Development of a Roll-to-Roll Apparatus

2.1. Introduction

In recent years, rapid development of organic materials has been drawing people's attention to the bright future of organic electronics. Organic materials normally have inferior electrical conductivity and durability to inorganic materials and it has been resisting the commercialization of organic devices despite the attractive features of them. However, developed organic material processing technologies, discovery of new materials like graphene, and the packaging technologies have enabled organic material based devices to make the best use of its advantages [7], [45], [46]. The benefits of organic material based devices are listed as follows: Devices can be flexible, stretchable, transparent, cheap, light, environment-friendly, and produced in a large scale.

The roll-to-roll manufacturing system is a suitable system for printed electronics fabrication. Since most of organic materials are processed in solution phase, printing technologies for text and graphic have started to be utilized for printed electronics. Conventional graphic printing technologies such as screen printing, gravure printing, flexographic printing, inkjet printing, and various coating methods are all capable of printing electronics. Those printing methods are able to be combined and work together in one roll-to-roll manufacturing system, and this goes along well with the cost-effective features of printed electronics, providing high and continuous throughput. Frederik C. Krebs developed a polymer solar cell roll-to-roll fabrication system in which flexography printing, slot-die coating and rotary screening printing are combined in one roll-to-roll system [47]. As seen in Frederik C. Krebs' system (Figure 2.1), a roll-to-roll system has many rollers to convey a web and to transfer ink and is compatible even with ovens, implying further more applications available with the roll-to-roll system.

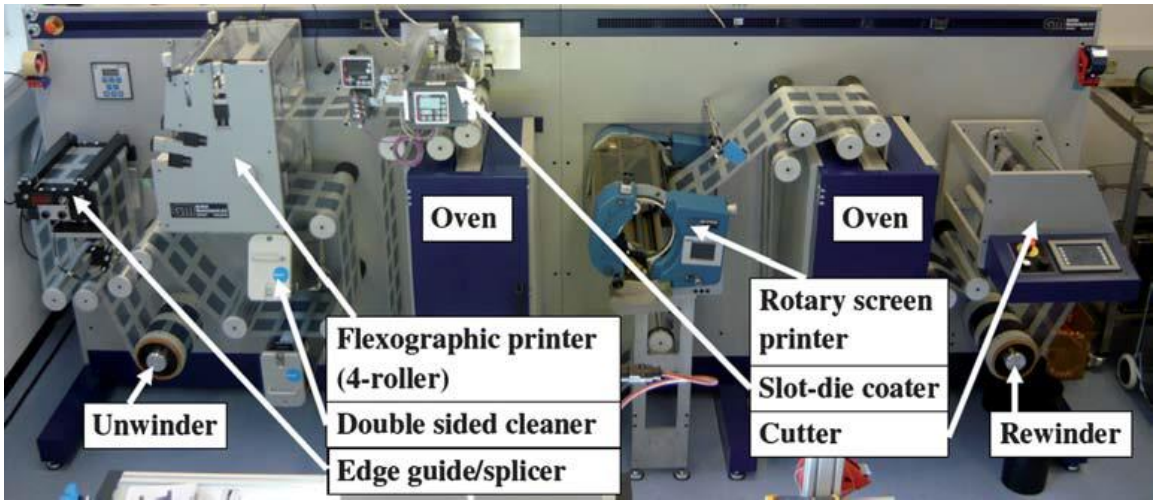

Figure 2.1. Polymer solar cell fabrication roll-to-roll system with three different printing and coating methods [47]. Reprinted with permission.

Jiseok Kim et al.[48] from Stretchable Device Lab at SFU demonstrated a roll-to-roll system for a flexible and strechable strain sensor fabrication where spray and Ultraviolet (UV) curing system are equipped to ink the stamp and to cure UV-curable adhesive layers (Figure 2.2).

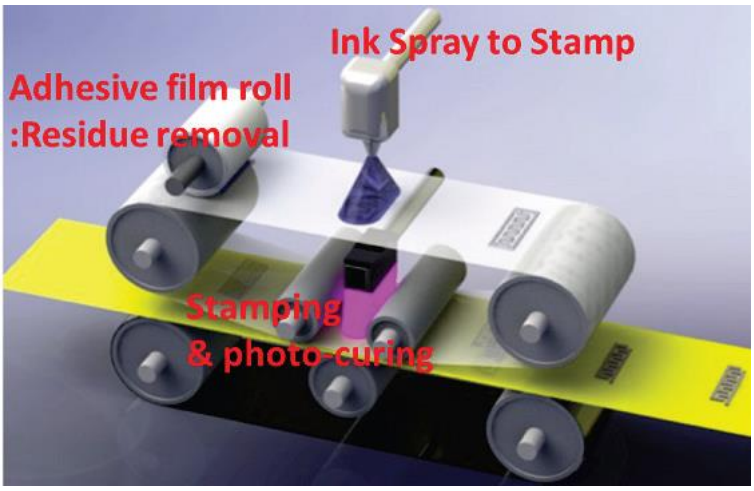

Figure 2.2. Conceptual design of a strain sensor fabrication roll-to-roll system equipted with spraying and photo-curing systems[48]. Reprinted with permission.

Likewise, many different materials can be printed by variety printing methods in one roll-to-roll system producing thousands of the printed electronics.

In this study, a roll-to-roll apparatus was built to develop a dry transfer technology (shear-induced transfer) for r-GO thin films that can be integrated into the roll-to-roll printed electronics manufacturing system. In general roll-to-roll systems, different rollers rotate at the same tangential speed to convey a long flexible substrate continuously without shrinkages or stretches. However, our apparatus was designed to be able to have different tangential speeds to induce shear strain on the stamp.

2.2. Development of Roll-to-Roll Apparatus

2.2.1. Specification of Roll-to-Roll Apparatus

A roll-to-roll apparatus for shear-induced transfer was designed and fabricated with acrylic glass sheets, 3 rollers, two step motors, sprockets, chains, a motor driver board, and a power supply. Acrylic glass sheets of 5.2mm thick were selected to form main frame structures because of its rigid and transparent properties as well as its easy fabrication method. Acrylic sheets were cut by a laser cutter (VLS 3.6, Universal Laser system), and were assembled using bolts, nuts, and L-brackets. Two rollers (AB-3601, LITH-O-ROLL) of 31.75mm in diameter were separately motorized by two step motors (23HS7430, Longs Stepper Motor) to accurately control each roller independently, and the third roller was placed little apart. The distance between the two motorized rollers can be adjusted to control vertical deformation of the stamp. The roller on the front side is installed on shaft holders (roller gap controller in Figure 2.3(b)) on each side which are movable back and forth. A vernier caliper is used to accurately adjust the distance between rollers. The rotation of motors is transmitted to rollers by metal chains and sprockets. Sprockets were 3-dimension (3D) modeled by Unigraphics NX5 (Figure 2.4(a,b)) and printed out by a 3D printer (Rostock max, SeeMeCNC) using a poly lactic acid (PLA) filament, a strong polymer material normally used for gears (Figure 2.4 (c)). A motor driver board (TB6560, TOSHIBA) was mounted on the frame (Figure 2.3 (b)) and connected to front two motors and a computer. This controller board is capable of controlling up to three step motors separately with 1/16 micro-step setting providing smooth and accurate rotation at low RPM.

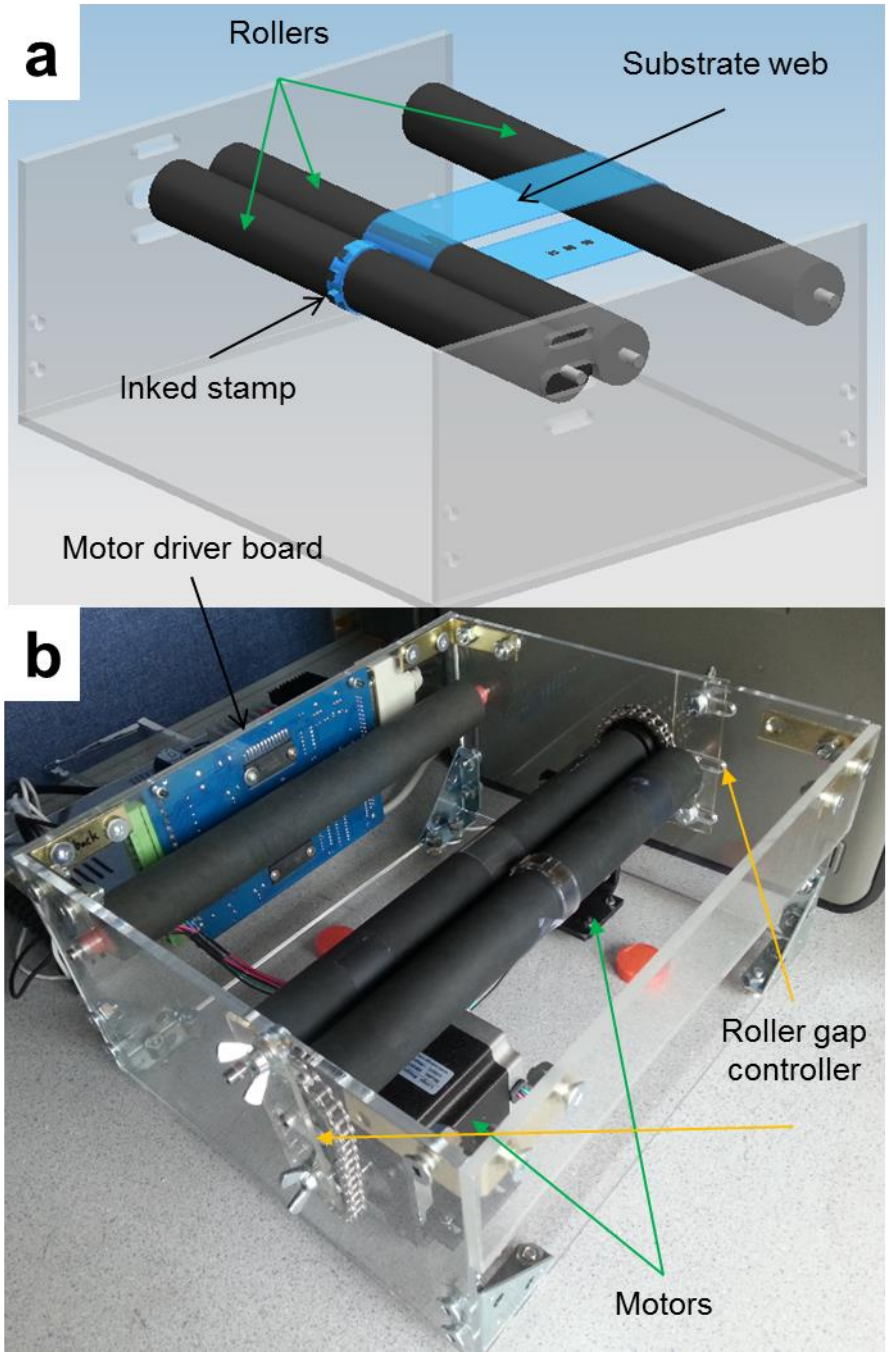

Figure 2.3. **(a) Schematic representation of the roll-to-roll apparatus for the array of rollers and the stamp. (b) actual fabricated apparatus with its all components.**

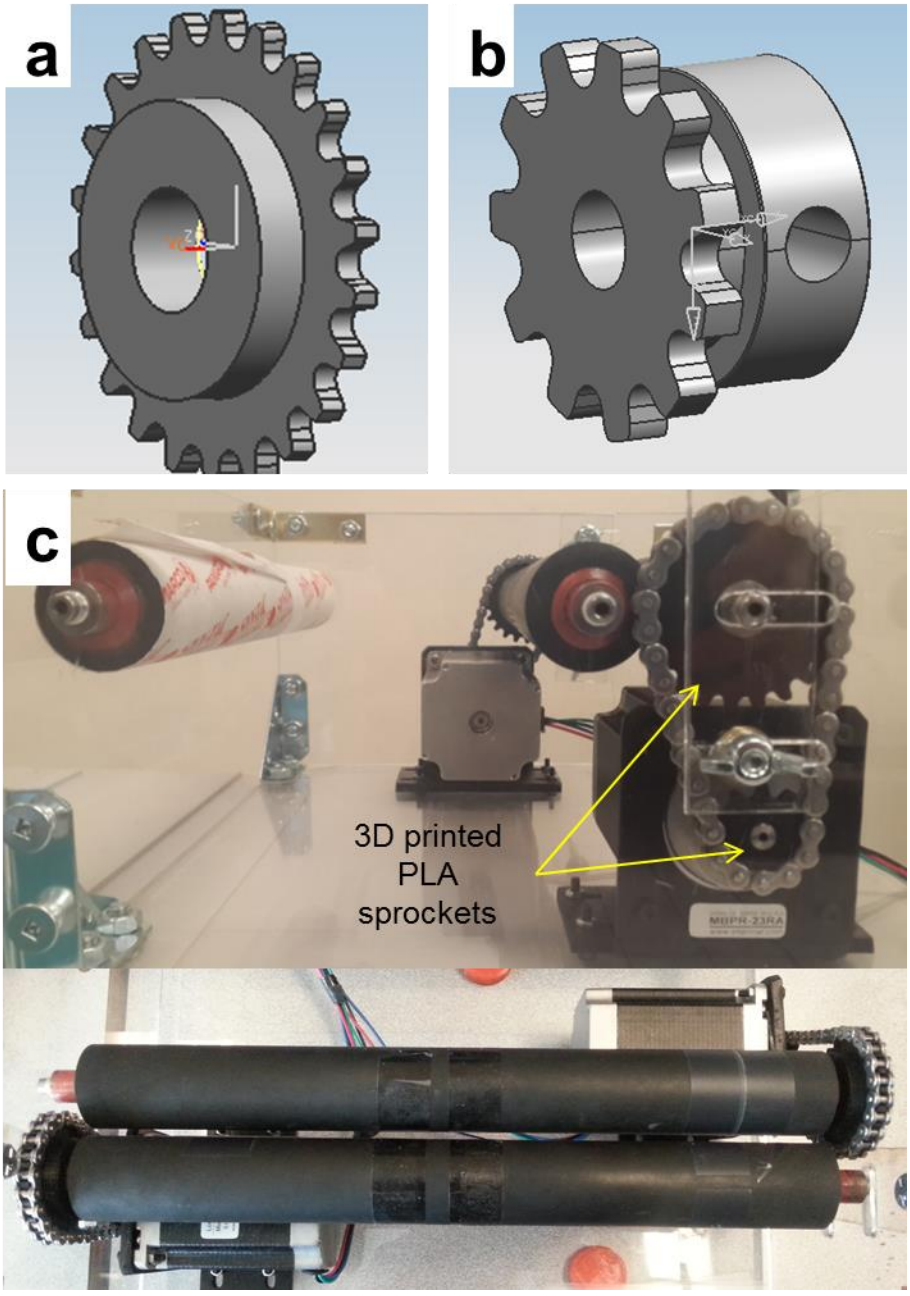

Figure 2.4. **3D modeled sprocket for (a) rollers and (b) motors. (c) side view (upper) and top view (lower) of the roll-to-roll apparatus with 3D printed sprockets.**

2.2.2. Control of Roll-to-Roll Apparatus

MACH3 software from Artsoft was installed in the computer to control the rollers by commands. It is easy to stop and run the motors repeatedly with MACH3 because it has an immediate stop button and works based on commands, while it also has manual control buttons. Since MACH3 was originally designed to control CNC machines, the interface is arranged to control rotating axes (X, Y, and Z) and the axes are controlled by G-code. Thus it is essential to first understand CNC machine control little bit. G-code is a programming language to move the machining tool according to its instructions. Instructions such as how fast and where to move are commanded by this language. While the software controls over three step motors, our system need only two motors. Therefore, one axis (x-axis) was chosen not to be used.

There are only three commands (codes) which are necessary for our system: G (basic moving type selection in CNC machining), Y and Z (coordinates of two axes), and F (speed). G is always set as ‘G01’ for linear motion. Y and Z are assigned to each roller and the ratio between the numbers typed after Y and Z indicate rotation ratio between them. F adjusts rotation speed of all axes. For example, if a command ‘G01 Y01 Z10 F50’ is given, Z roller rotates 10 times faster than Y roller and the RPMs of the two rollers are proportional to F value (50 here), and the given rollers’ speeds do not change until rollers stop because of command ‘G01’.

The RPM of the two rollers at G-code commands was calibrated through tests in order to be able to accurately control the rollers using G-code. The calibration was done when the gear ratio between the roller and the motor is 2:1, and the micro-step setting is 1/16. When Y and Z are the same and F is 50, rollers rotate 360˚ in 0.95 second. Based on the calibration data, an Excel file was programmed to calculate G-code command values with respect to the RPM and RPM ratio required for experiments. Figure 2.5 shows the software interface window and calculated G-code values in an Excel table. G-code values are calculated based on the RPM and RPM ratio input (yellow boxes). G-code values presented in Figure 2.5 are for when the RPM of the substrate side roller is 0.05 and the stamp side roller is 1.4 times faster.

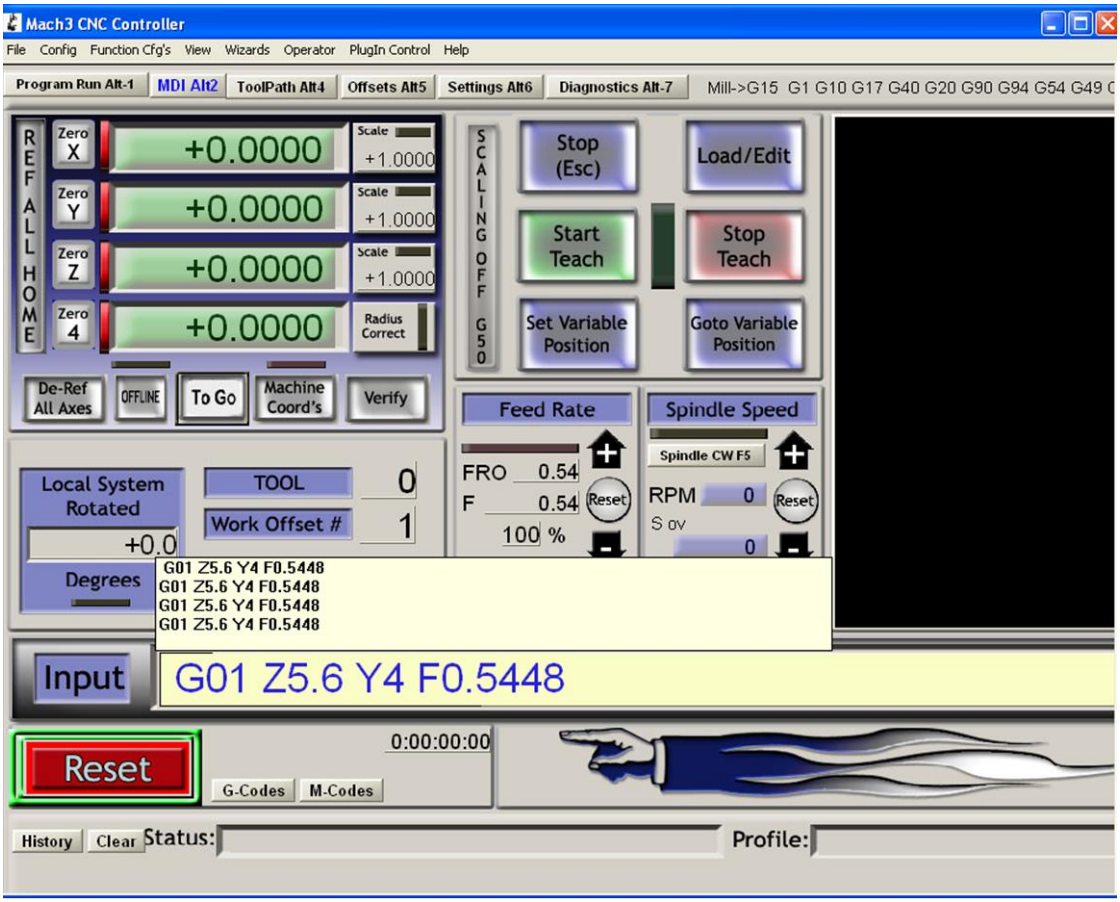

Z	Y	F	RPM(Z)	RPM(Y)	RPM ratio
5.6	4	0.544814	0.07	0.05	1.4

Figure 2.5. MACH3 software interface window (upper) and an Excel table for G-code calculations (lower).

Chapter 3.

Shear-Induced Roll-to-Roll Transfer

3.1. Objective and Plan for the Transfer Experiments

In this chapter, shear-induced transfer is explained with experiment results followed by the r-GO thin film preparation method section. A post-treatment for the transferred r-GO thin film is also investigated for optimizing the electrical property of the film (Figure 3.1).

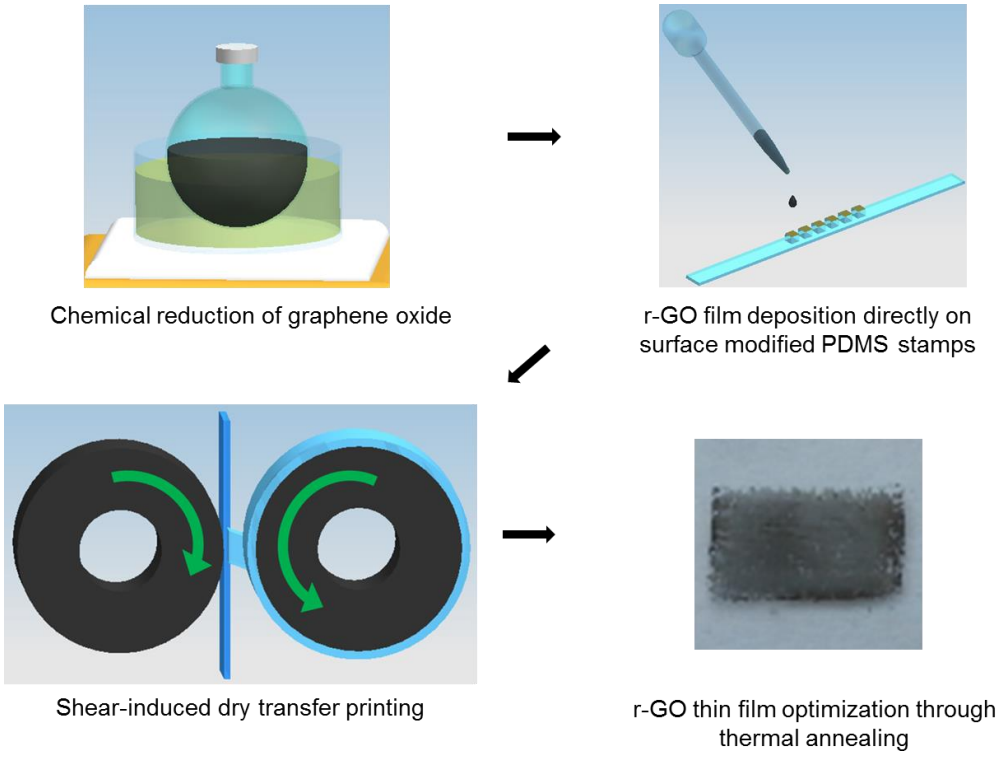

Figure 3.1. Process flow of transfer experiment. Prepared r-GO solution is drop-cast on surface modified PDMS stamp to form r-GO thin film followed by shear-induced transfer onto the target substrate and a post-treatment process.

Among many different graphene material preparation methods, solution processed chemical reduction of graphene oxide has been chosen for our film material. As explained earlier in chapter 1, this method enables large scale production of r-GO at room temperature without vacuum condition and post-treatments like etching process in CVD based graphene preparation system. Though solution processed r-GO has less electrical conductivity, it is much cheaper to produce in a large scale and has as many applications as CVD grown graphene [49].

Transfer printing has been selected as our transfer method to transfer r-GO thin films. Transfer printing with PDMS stamp, a common stamp material for its ability to make a conformal contact, has advantages in its simplicity, ease of creating micro-size patterns, and compatibility with Roll-to-Roll manufacturing system. Stamps can be easily fabricated multiple times from a single master and individual stamps can be used repeatedly. It is a cheap technic for fabrication which uses less energy because it does not require high temperature and a clean room.

There is one group, Matthew Allen et al.[50] that used transfer printing with PDMS stamps to print chemically reduced graphene oxide on a silicon wafer. They deposited r-GO on an oxygen plasma treated glass substrate using spin coating followed by a thermal annealing process and inked the PDMS stamp by simply putting the stamp on the prepared r-GO thin film and then transferred on to a silicon wafer in the same way but with much longer time and raised temperature. The transfer process is illustrated in Figure 3.2. The mechanism used in their printing process is based on differing strength of van der Waals' force in the interfaces. When PDMS stamp is brought into contact with a r-GO thin film on a glass substrate, the hydrophobic surface of r-GO tends to have stronger van der Waals' interaction with the hydrophobic surface of PDMS than it does with the hydrophilic surface of the glass surface. The transfer from the glass substrate to PDMS stamp takes place in about 2 minutes, while still not the whole stamp surface is inked with r-GO as shown at the right side of Figure 3.2. Transferring r-GO thin film from the stamp to a silicon wafer is even harder. Several days of contact time is necessary to transfer r-GO thin film from the stamp to a silicon wafer at room temperature. With the raised temperature to 75˚C, the required contact time decreases down to 30 minutes. The mechanism applied here is based on dissociation of low molecular weight

oligomers from the PDMS surface [51][52]. As the oligomers are dissociated from the PDMS surface, r-GO thin film on the surface is released and this happens faster at higher temperature but 30 minutes is still not a short time. Since the transfer occurs because of the dissociation of the oligomers, only freshly prepared PDMS can be used meaning stamps cannot be used multiple times and this is another big drawback of this transfer mechanism.

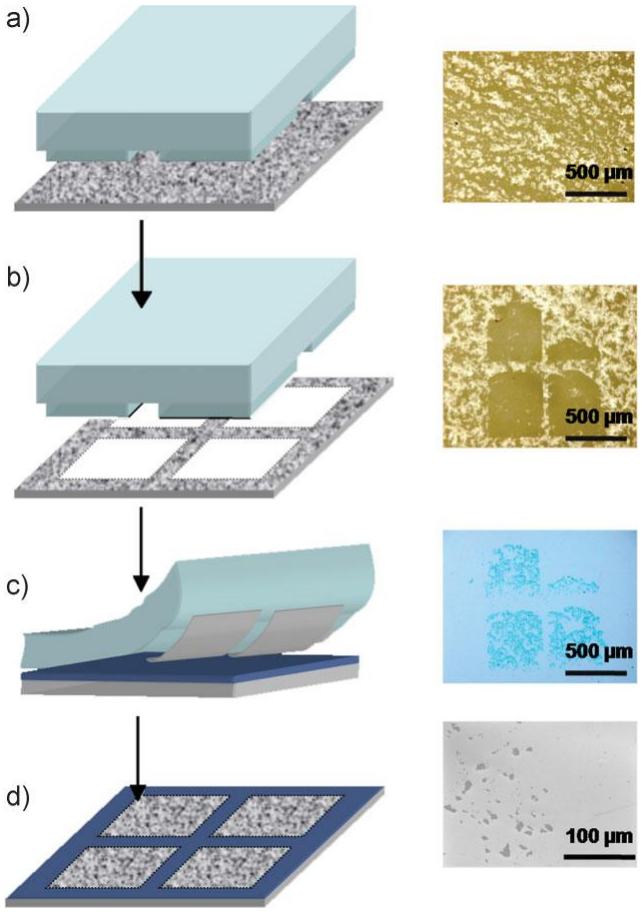

Figure 3.2. Schematic illustration of transfer printing (left) and microscopic pictures (right). a) r-GO deposition on a glass substrate. b) inking PDMS stamp with r-GO thin film. c) contact with Si/SiO_2 substrate. d) peeling the stamp off [50]. Reprinted with permission.

Our shear-induced transfer printing is a very simple process that uses neither additional energy sources nor chemicals, not to mention adhesive. r-GO thin film deposited on the stamp is transferred onto the target substrate assisted by applied shear stress on the stamp surface. The roll-to-roll printing apparatus explained in chapter 2 was used to conduct transfer experiments to demonstrate transfer printing in a roll-to-roll

manufacturing system. The shear strain on the stamp post is induced by rotating the stamp side roller faster than the substrate side roller (Figure 3.3). The mechanism will be discussed in detail in **3.2** Theoretical and Computational Analysis of Shear-Induced Transfer. r-GO thin film is prepared on the surface of PDMS stamp directly by dropcasting. The direct deposition of solution processed r-GO on the PDMS surface is known to be very hard due to the hydrophobic surface of PDMS, but the surface modification process with polydopamine enables the deposition by changing the surface property to hydrophilic. Thanks to the stamp surface modification process, our printing system has one transfer step from the stamp to the substrate rather than two like Matthew Allen et al. [50] did. The transferred r-GO thin films are put into a post-treatment process to evaporate solvent molecules trapped in the thin films and to remove residues from the stamp surface. After the post-treatment step, the electrical property of the thin films is greatly improved.

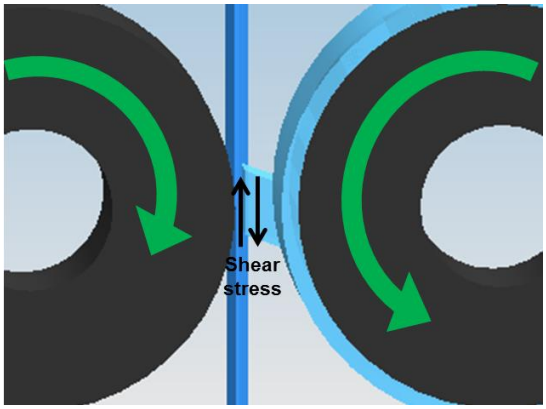

Figure 3.3. Shear stress induced on the stamp surface by different roller speeds. The stamp side roller rotates faster than the substrate side roller.

3.2. Theoretical and Computational Analysis of Shear-Induced Transfer

Griffith's fracture analysis is considered for the analysis of our r-GO thin film transfer between two rollers. Griffith employed energy-balance approach in facture analysis and that became one of the most famous developments in materials science [53]. To determine fracture or film delamination behaviour in the perspective of the energy based analysis, the work required to separate the surfaces is compared to the strain energy released as a crack grows [54]. The work required to separate a thin film

from the substrate per area is defined as interfacial toughness. Strain energy release rate is the energy applied on the interface to separate the surfaces per area. In the ideal case of Griffith facture, the interfacial toughness is equal to thermodynamic work of adhesion [55]. In reality, however, even brittle materials' fractures are accompanied by energy dissipation through plastic deformation at the crack tip or friction. Therefore, interfacial toughness of a film and the substrate is defined as

$$\Gamma_{(\psi)} = W_A + U_f + U_s + U_{fric} \qquad (1)$$

where $\Gamma_{(\psi)}$ is interfacial toughness or energy per area required to delaminate the film with respect to mode mixity which is a relative measure of the amount of shear and normal stress components ($\Psi = \tan^{-1}(\tau/\sigma)$), W_A is thermodynamic work of adhesion, which is the adhesion work of polydopamine in our case because polydopamine is decorated on the stamp surface before r-GO thin film deposition and it is in contact with r-GO thin film, U_f and U_s are the energy spent in deformation of the thin film and substrate, and U_{fric} is the energy loss due to friction [56]. Interfacial toughness is also regarded as the resistant to the crack propagation and strain energy release rate is the crack driving force (delamination driving is regarded as crack). Therefore, strain energy release rate should be bigger than interfacial toughness for film transfer to occur:

$$\mathrm{G} = -\frac{\partial(U-V)}{\partial A} \geq \Gamma_{(\psi)} = R \qquad (2)$$

where G is strain energy release rate, U is potential energy available for crack growth, V is work associated with any external forces, A is crack area, and R is the resistant to the crack propagation [55][57]. To have the film transfer happened, and to have enough strain energy release rate in order to overcome the interfacial toughness between the film and stamp, in other words, the total amount of strain release rates by different loads should be investigated. In transfer printing, strain energy release rate is usually driven by the pulling force exerted on the film to peel it off. In our case, the pulling force is determined by the van der Waals' interaction between the r-GO thin film and the substrate surface when those are in contact. Since the r-GO thin film is drop-cast on the polydopamine modified stamp surface, the film has stronger interaction with the stamp

than with the substrate. Thus, transfer does not happen if it is only with the pulling force. As shown in equation $G_{total} = G_1 + G_2$ (3)

$$G_{total} = G_1 + G_2 \quad (3)$$

where G_1 and G_2 are strain energy release rates by mode 1 and 2 loads (mode1: opening (Figure 3.4(a)), mode2: sliding (Figure 3.4(b))), total strain release energy is the sum of those two [58]. To have the total strain energy release rate exceed the interfacial toughness, different load modes have to cooperate. In our shear-induced transfer printing, mode2, sliding mode, was applied in addition to mode 1 to increase the energy exerted on the interface by making the stamp side roller rotate faster as explained in previous section.

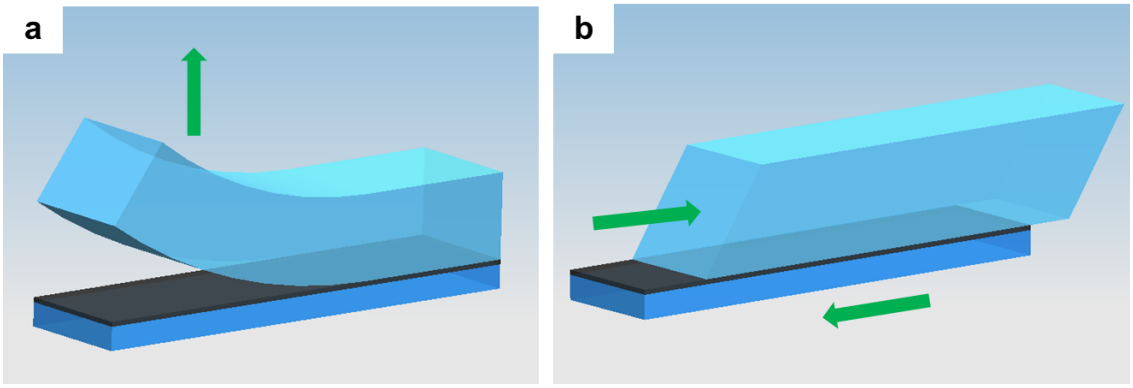

Figure 3.4. Illustration of the r-GO thin film transfer by (a) pulling force (mode1) and (b) shear force (mode2). Two different modes can be applied together to facilitate transfer.

As found in Figure 3.25 Figure 3.26, r-GO thin films were transferred onto the glass substrates when RPM ratio is 1.4 or higher. It seems RPM ratio of 1.4 shows the best result considering the wrinkles and cracks on the films. In the higher RPM ratio than RPM ratio of 1.4, the excess energy induced by shear force is used to cause wrinkles and cracks on the transferred r-GO thin film. Figure 3.5 shows how critical interfacial toughness changes as the mode mixity angle increases. Critical interfacial toughness is the lowest when only mode1, pulling force, alone is applied. However, mode2, sliding force or shear force, has to be added inevitably to have higher strain energy release rate because the pulling force from the target substrate is insufficient to overcome the critical interfacial toughness. As the portion of mode 2 becomes bigger, the critical interfacial

toughness gradually increases and reaches to the maximum when mode2 alone is applied. While critical interfacial toughness increases, the thermodynamic work of adhesion remains constant, meaning there is energy dissipation as much as the energy difference between them. The energy is dissipated through energy loss by friction, damages on the transferred r-GO thin film, and the elastomeric rubber stamp (equation ($\Gamma_{(\psi)} = W_A + U_f + U_s + U_{fric}$ (1)) and this is a drawback of this shear-induced transfer because there should be higher energy dissipation always when shear stress is used. Therefore, it is very important to find an optimal point where the use of shear force is the minimum, while the critical strain energy release rate is attained.

To quantify the required shear force in this thin film transfer condition, the shear stress on the stamp surface was calculated by experimental measurements and ANSYS simulation software. The lateral direction displacement of the stamp post is equal to the tangential speed difference of two rollers multiplied by the contact time assuming the effects by the curvature are negligible. The contact time of the stamp surface and the substrate when the RPM of the substrate side roller is 0.05 was measured three times each by video recordings and averaged (Figure 3.6). The contact time should be the same regardless of RPM ratio in theory because the stamp surface is in contact with the substrate until the substrate moves enough to release the stamp, but in reality the contact time decreases as RPM ratio increases because of the effect of stamp deformation. The tangential speed is calculated based on RPM, the roller radius (31.75mm), the stamp thickness (2.6mm) for the stamp side roller, and the substrate thickness (1mm) for the substrate side roller as shown in the equation below.

$$V_t = r \times \omega = (r_R + h_s) \times \frac{RPM}{60} \times 2\pi \qquad (4)$$

where V_t is tangential speed, r is radius, ω is angular speed, r_R is radius of roller, and h_s is height of stamp or substrate. Lateral displacement is calculated with the equation below.

$$Lateral\ displacement = (V_{stamp} - V_{substrate}) \times contact\ time \quad (5)$$

where V_{stamp} is tangential speed at stamp surface and $V_{substrate}$ is tangential speed at substrate surface.

The calculated lateral displacements of the stamp surface are shown in Figure 3.7(b).

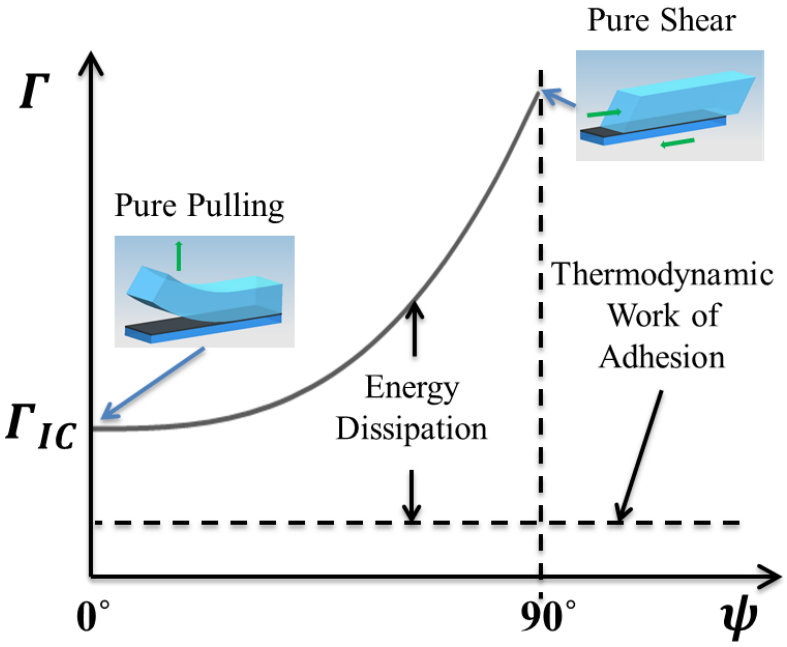

Figure 3.5. Critical interfacial toughness as a function of mode mixity angle [55]. As shear portion increases, critical interfacial toughness increases. Adapted with permission.

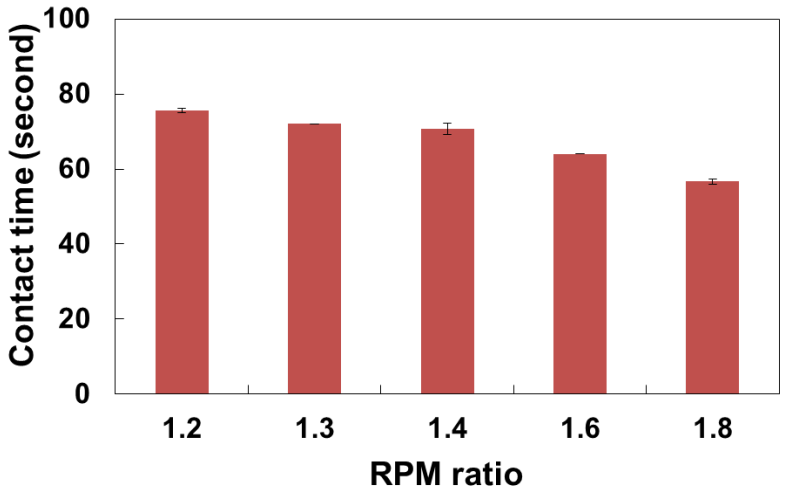

Figure 3.6. **Stamp contact time according to RPM ratios. The contact time decreases as RPM ratio increases.**

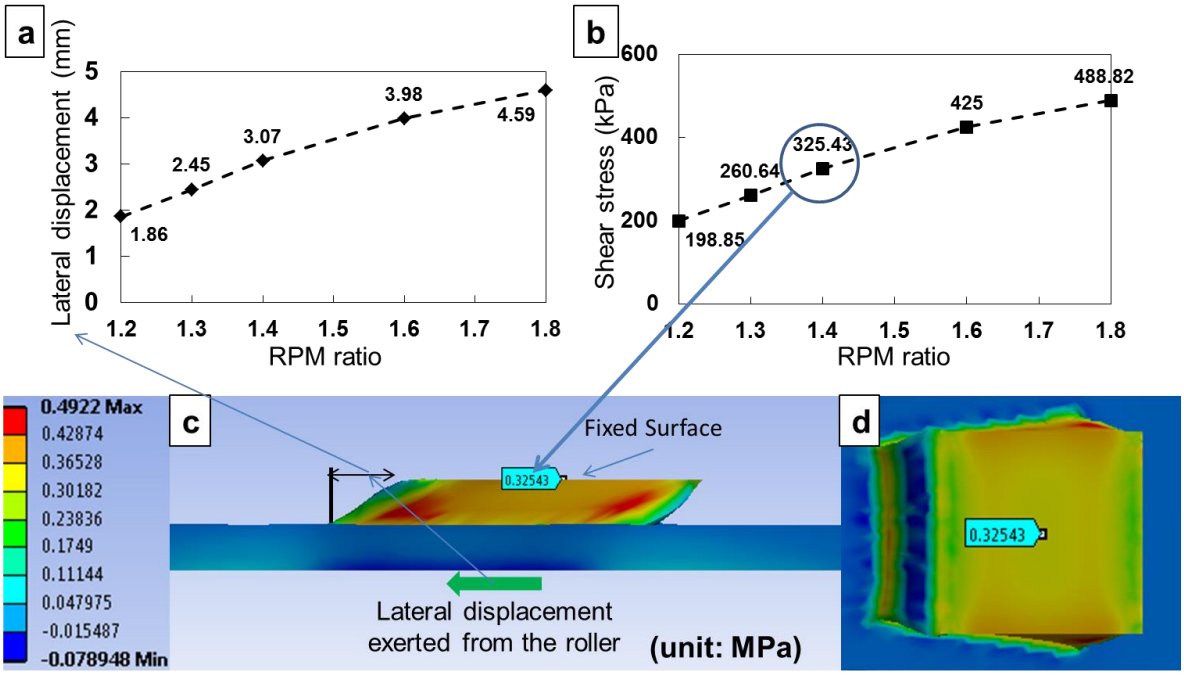

Figure 3.7. **(a) Lateral displacements of the stamp post according to different RPM ratios. (b) Simulated shear stress values with respect to RPM ratios. ANSYS simulation results: (c) side view with applied simulation condition and (d) top view (at RPM ratio of 1.4).**

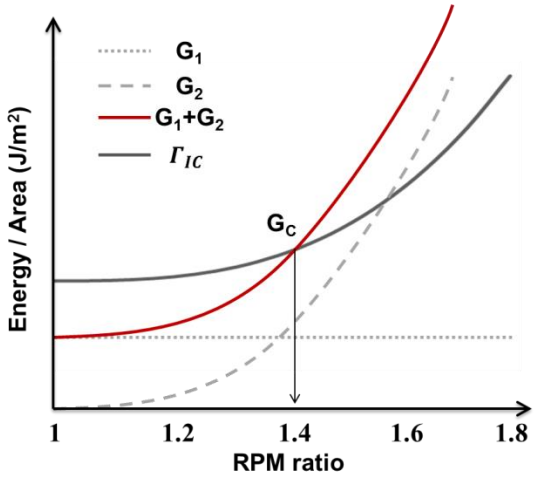

Figure 3.8. Critical interfacial toughness and total strain energy release rate according to different RPM ratio. As RPM ratio increases, G_1 remains constant G_2 increases thus increasing the total G value. G_C is critical strain energy release rate from which the film can be separated from the stamp.

Assuming the effects that come from the curvature of the roller are negligible, calculated displacements were put into ANSYS simulation software as shown in Figure 3.7(c) to simulate induced shear stress on the stamp surface with respect to RPM ratios (Figure 3.7(b)). Shear stress distribution in stamp is visualized from sideview (Figure 3.7(c)) and topview (Figure 3.7(d)). The material properties of the PDMS stamp that was set in the software are as follows: Yong's modulus: 2.7 MPa, shear modulus: 0.89 MPa, bulk modulus: 43.3 MPa, and Poisson's ratio: 0.49. It has been confirmed through experiments that RPM ratio of 1.4 is the point from which the transfer happens. According to the experiment results and simulation results, the shear stress that has to be induced on the stamp surface for film transfer is 325.43 KPa.

Strain energy release rate is proportional to the square of normal stress (for G_1) or shear stress (for G_2) as shown below [59].

$$G_1 \fallingdotseq \frac{\sigma^2 \pi a}{E},\ G_2 \simeq \frac{\tau^2 \pi a}{E} \quad (6)$$

Where σ is normal stress, τ is shear stress, a is crack tip length, and E is Young's modulus. As we explore experiments with different RPM ratios, G_1 remains constant because RPM ratio does affect pulling force onto the film, and G_2 increases

proportional to the square of the shear stress value calculated in Figure 3.7 (b). Figure 3.8 illustrates the relations that RPM ratio has with strain energy release rates and critical interfacial toughness. Without RPM ratio applied, the total strain energy release rate has no way to overcome the critical interfacial toughness. By adding shear strain release rate by shear force (G_2), the total strain energy release rate can reach to critical strain energy release rate, from which the film is separated from the stamp, when RPM ratio is 1.4 as experimentally proven (refer to Figure 3.25).

3.3. Preparation of r-GO Deposited Stamp

3.3.1. Reduction of Graphene Oxide

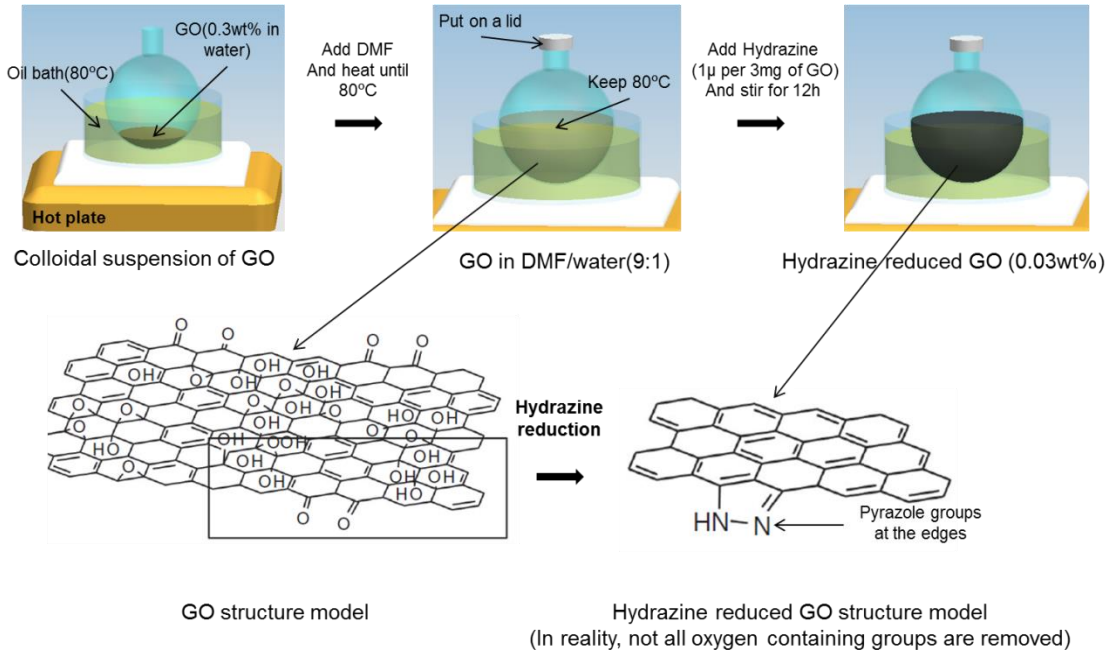

Figure 3.9. Schematic illustration of graphene oxide reduction process and the chemical structure changes (-COOH groups at the edges are omitted from the figure for clarity). Oxygen groups on the basal plane disappear after reduction and pyrazole groups are attached at the edges due to hydrazine[60]. Adapted with permission.

For the preparation of reduced graphene oxide, one of the most well-known methods has been chosen. Commercialized GO solution in water was purchased (0.5 wt. % GO, Angstron Materials Dayton, OH, USA) and was treated with hydrazine

monohydrate, a strong reduction agent, to eliminate oxygen functional groups (reduction). Detailed material preparation process is as follows [61]:

1. Heat silicone oil bath up to 80˚C on a hot plate.
2. Take 15ml of GO solution into a flask and add 10ml of water to have GO of 0.3wt % in water.
3. Sonicate the GO solution for 2h to make sure that there is no agglomeration.
4. Add 225ml of Dimethylformamide (DMF) to make it 9parts DMF and 1part water (in volume).
5. Put the flask into the oil bath and wait until the temperature is stabilized at 80˚C (keep stirring the solution using a magnetic bar).
6. Apply 38.5μl of 65% hydrazine monohydrate (pure 1μl for 3mg of GO).
7. Continue to stir for 12 hours at 80˚C with the flask plugged up.
8. Cool down at room temperature and have 5 minutes of sonication.

The r-GO solution in DMF/water solution produced by the method presented above is very stable colloidal suspension that has stayed more than a year without floating or precipitated particles.

To confirm the reduction of graphene oxide, Attenuated Total Reflextance Infrared Spectroscopy (ATR-IR) (L160000A, PerkinElmer) and Ultraviolet-Visible Spectroscopy (UV-Vis) (Cary 50, Varian) spectroscopy were used to characterize. In Figure 3.10, peaks at 230nm and 300nm were removed and a new peak at 264nm arose after the reduction process. This peaks' changes are a typical phenomenon as reduction of GO occurs, meaning reduction has been successfully done [22], [62].

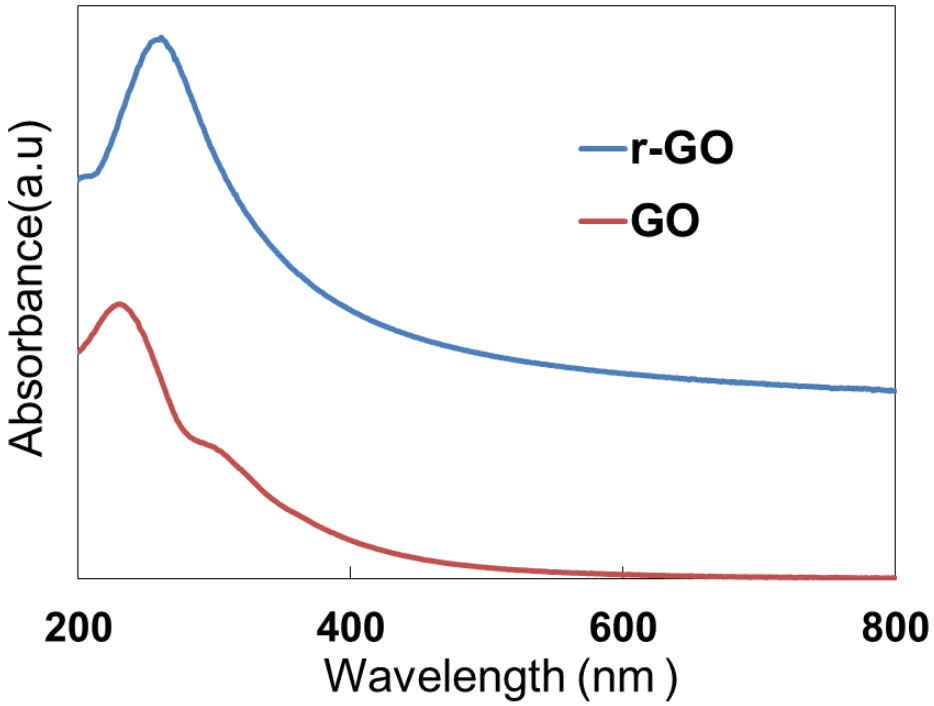

Figure 3.10. UV-Vis spectra of GO and r-GO.

The reduction of oxygen groups by hydrazine treatment was also confirmed using ATR-IR spectroscopy. In Figure 3.11, ATR-IR spectra of GO shows O-H (3395 cm^{-1}), alkoxy C-O (1069 cm^{-1}), epoxy C-O (1233 cm^{-1}), carboxy C-O (1414 cm^{-1}), C=C (1625 cm^{-1}), and C=O (1728cm^{-1}) stretches, which are common peaks arrangement for GO [62][63]. After hydrazine treatment, oxygen functional groups are scaled down considerably or removed, and two broad peaks at 1192^{-1}and 1560cm^{-1} appear. It is assumed that 1192cm^{-1} corresponds to the C-O stretch and 1560cm^{-1} to the aromatic C=C stretch [61]. Both UV-Vis and ATR-IR results confirm that our hydrazine treatment reduces GO as it is supposed to do. Though this reduction process restored the sp^2 network of graphene significantly by reducing functional groups, not all oxygen groups were disappeared as presented by ATR-IR characterization and it has been reported that reduction of GO with hydrazine monohydrate causes formation of pyrazole groups (aromatic five-membered rings with two adjacent N atoms) at the edges of r-GO platelets [60].

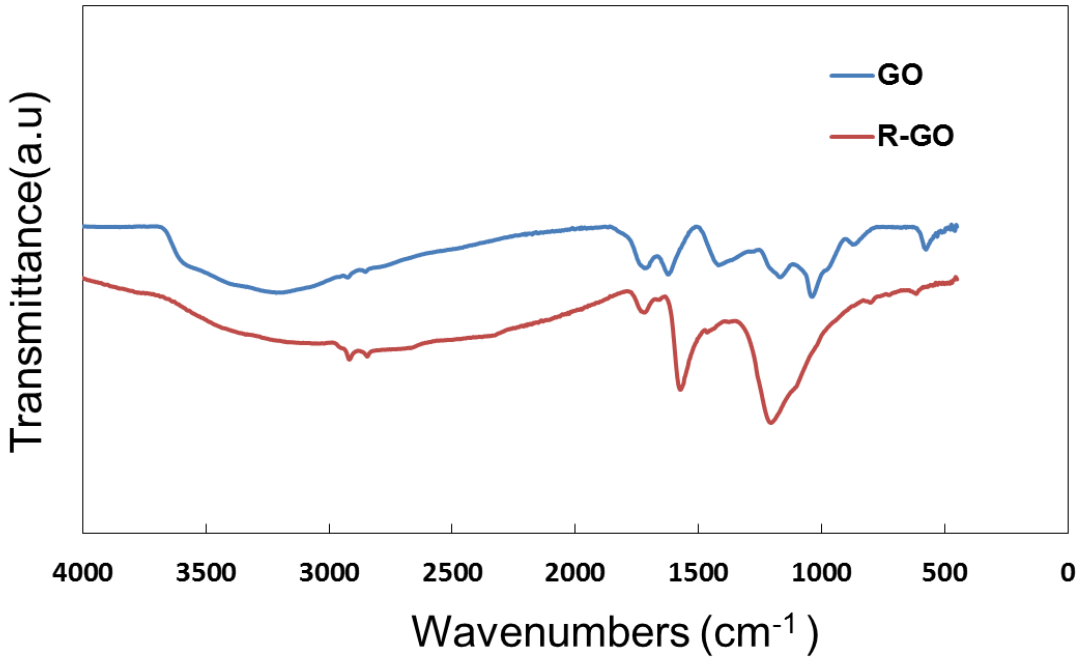

Figure 3.11. ATR-IR spectra of GO and r-GO.

3.3.2. Flexible Stamp Fabrication

The stamp for r-GO thin film transfer was design as shown in Figure 3.12(b). The stamp post is 8×8×1.3mm^3 in size and the back support part is also PDMS of 1.3mm thick which is designed to be long enough to wrap the roller. The stamp mold was first fabricated with laser cut plexiglasses of 1.3mm thick and Polyethylene terephthalate (PET) at the bottom. Plexiglasses were put together by adhesive and PET was attached on the bottom using a double sided tape (Figure 3.12). The stamp fabrication steps are as follows. Polydimethylsiloxane (PDMS elastomer, Sylgard 184) and cross-linker purchased from Dow Corning are thoroughly mixed at 10:1 ratio and the mixture is poured into the mold after air bubbles are removed in a vacuum chamber. The mold with PDMS in it stays in an oven at 65 ˚C for an hour to cure the PDMS and the cured stamp is gently unmolded manually.

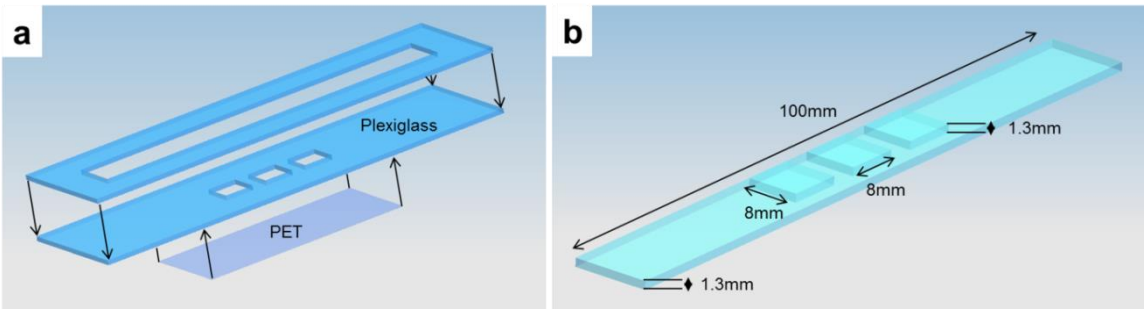

Figure 3.12. (a) Laser-cut plexiglass mold for stamp roll fabrication, (b) stamp dimensions.

3.3.3. Stamp Surface Modification by Polydopamine

The surface of the PDMS stamp has to be modified in order to evenly deposit r-GO thin film on the surface by dropcasting. PDMS is a hydrophobic material in which water and DMF are not able to spread evenly on the surface. Figure 3.13(a) is the case when r-GO solution is drop-cast on a bare PDMS. To make the stamp surface hydrophilic, polydopamine modification method was chosen. Haeshin Lee et al.[64], inspired by the mussel's great adhesion on almost every substance, researched on the composition of adhesive proteins in the mussel and found a way to coat multifunctional polymer layer on a wide range of materials. The coating method developed by Haeshin Lee et al. was able to coat even PDMS surface with polydopamine making the surface hydrophilic due to O-H groups of polydopamine.

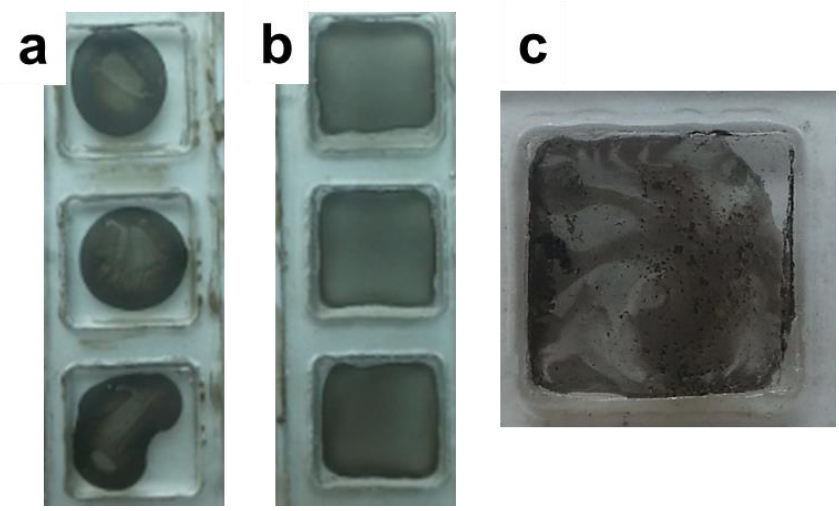

Figure 3.13. Pictures of r-GO thin films drop-cast on (a) bare PDMS and (b) polydopamine modified PDMS. (c) r-GO thin film deposited on a stamp after the stamp was once used for a transfer. Polydopamine surface modification enables even deposition of r-GO thin film.

The surface properties of the PDMS stamp are dependent on the parameters in the modification process. The PDMS surface modification process consists of three big steps: 1. Dopamine solution preparation, 2. Soaking PDMS in the solution, 3. Rinsing in flowing DI water and Drying in air (Figure 3.14). Three parameters considered in this thesis are the concentration of dopamine hydrochloride (Aldrich) in the solution, temperature, and the soaking time. As the dopamine concentration increases, the polydopamine layer becomes thicker also making the surface rougher [64][65][66]. Raising temperature makes the self-polymerization of dopamine monomers faster, resulting in smaller polydopamine particles deposited on the surface [67]. Though small particles grown at high temperature can be aggregated forming big clusters, deposition of those clusters can be prevented by placing the stamp upside down in the solution(Figure 3.14(b)) and by rinsing with DI water after coating [66]. The thickness and roughness of polydopamine layer is proportional to the reaction time [64][66]. The roughness of polydopamine modified PDMS was explored using AFM scanning (NX-10, Park Systems). The data shown Figure 3.15 endorses the relation between modification time and the roughness. The shorter the PDMS is in the solution, the less rough the surface is. For the purpose of the deposition and contract pringting of r-GO thin film, the modification step should ensure that polydopamine on the stamp does not create a rough surface, implying that the polydopamine layer on the stamp needs to be thin, as

long as the surface is hydrophilic enough to evenly deposit r-GO thin film, to minimize roughness. Therefore, low concentration (1g/l) of dopamine in the solution, high temperature (60˚C), and short modification time (15min) were selected. Combining studies on the parameters, our dopamine modification method was developed as follows.

1. Dissolve 0.12119 g of tris (hydroxymethyl) aminomethane (Sigma-Aldrich) in 50ml of DI water.
2. Add Hydrochloric acid (HCl) (37%, Aldrich) until pH becomes 8.5.
3. Pour 50ml of water additionally and heat it until 60˚C.
4. Dissolve dopamine hydrochloride (Aldrich) of 0.1g.
5. Put the stamp sample upside down in the prepared solution while keeping 60˚C.
6. Take the sample out after 15 minutes and rinse with flowing DI water.
7. Dry the surface with an air gun.

The reaction time longer than 15minutes did not make big differences in contact angle (measured by Digital AST Contact Angle System) unless it is 24hours (contact angle after 24hours=72˚) (Figure 3.16). It was experimentally verified that modification time of 15minutes is enough to evenly deposit r-GO thin film on the surface as shown in Figure 3.13(b). In addition, the r-GO thin film transfer results with different modification time in Figure 3.17 prove benefits of having short modification time. The poorer transfer results seen in the samples with longer modification time are ascribed to higher roughness because higher roughness ends up with smaller contact area with the substrate, thus having weaker adhesion to the substrate. Therefore, the modification time needs to be kept short.

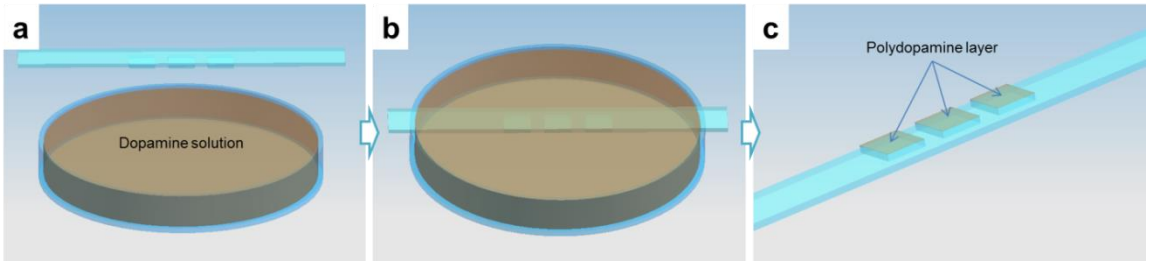

Figure 3.14. Schematic illustration of stamp modification process: (a) dopamine solution preparation, (b) stamp soaking in the solution, (c) rinse with DI water and air dry. The stamp is covered with polydopamine layer after this process.

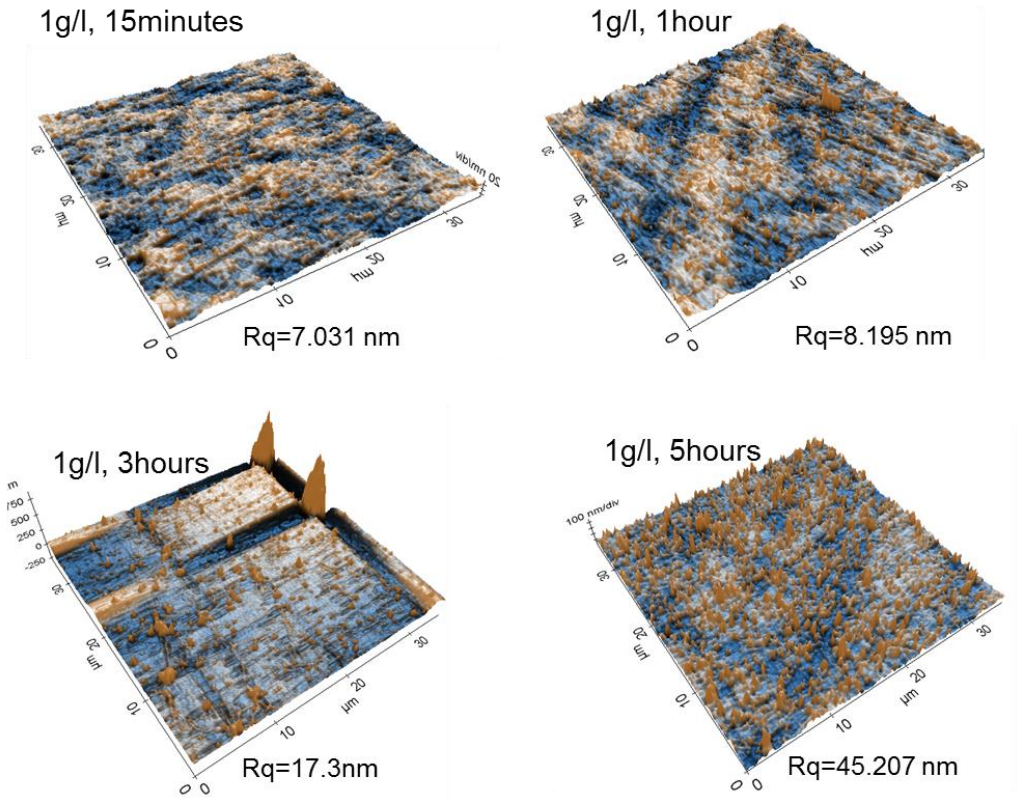

Figure 3.15. AFM scan images and roughness (root mean squared) of polydopamine modified PDMS surfaces with different modification time. Longer modification time makes the surface rougher.

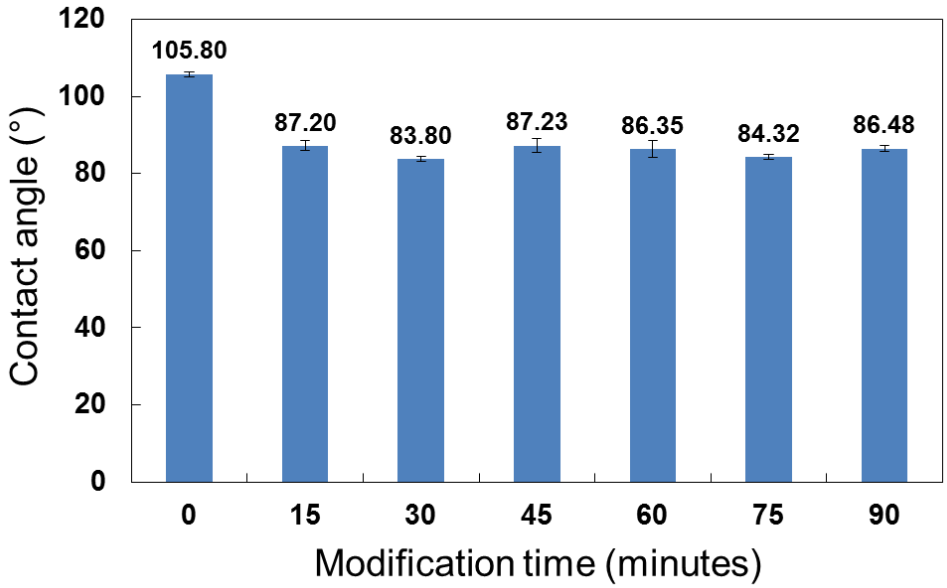

Figure 3.16. Contact angle measurement of polydopamine modified PDMS surfaces. Contact angle does not change significantly after 15 minutes.

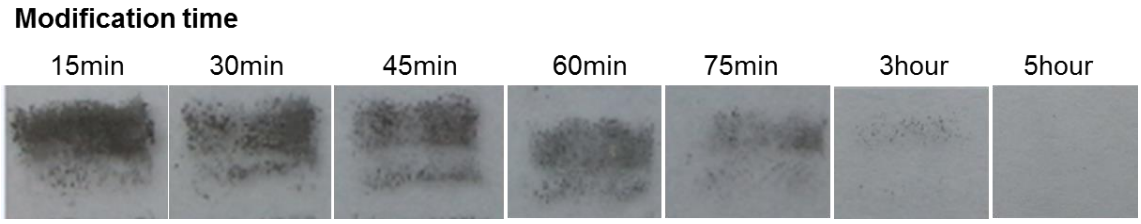

Figure 3.17. Dopamine modification time and the corresponding results of r-GO thin film transferred onto glass substrates (before other parameters were adjusted). Longer modification time hinders transfer of r-GO thin film.

3.3.4. r-GO Deposition on Stamp

Thanks to polydopamine modification, r-GO thin film can be formed on the stamp surface by dropcasting, the simplest and economic method. r-GO solution (0.03wt%) of 0.3875 $\mu l/mm^2$ (24.8 μl for our stamp) is drop-cast on the modified stamp surface. Evaporation of solvents is enhanced by drawing vacuum. Vacuum level of -0.096MPa has been used. Evaporation time in the vacuum chamber as an experiment parameter is discussed in 3.4.1.Optimization of Dropcast. Transmittance of the drop-cast film was measured by UV-Vis spectroscopy and the transmittance at wavelength of 550nm was

40% as shown in Figure 3.18. Our film has low transparency, whereas there are graphene films with transparency of higher than 90%. The transparency can be improved by reducing amount of r-GO solution during dropcasting deposition. However, this thesis focuses more on film deposition itself and the transfer process, leaving that issue as a future work.

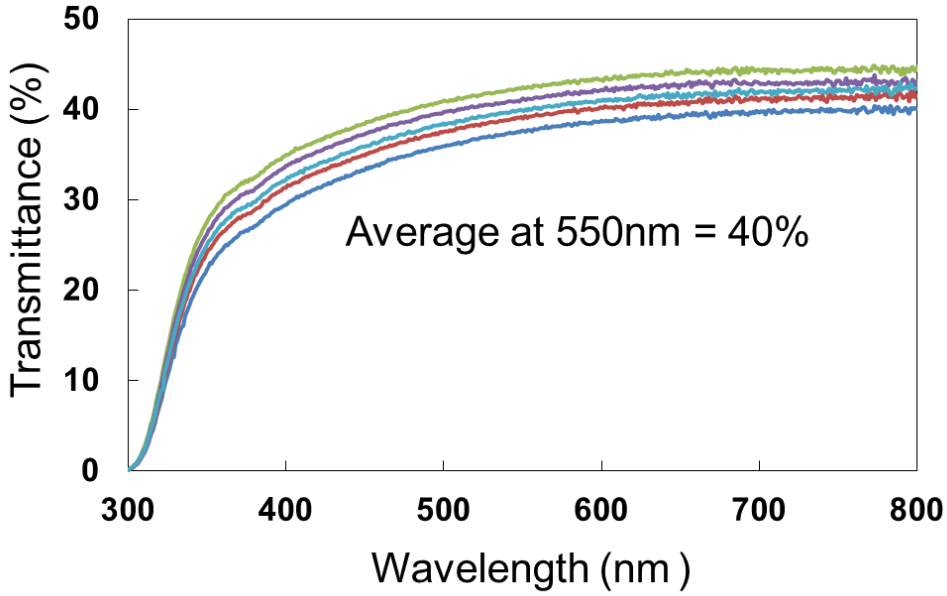

Figure 3.18. Transmittance of drop-cast r-GO thin films (when 0.3875µl/mm^2 of r-GO solution (0.03wt%) was drop-cast). Transmittance at 550nm wavelength is 40%.

3.4. Optimization of Transfer Parameters

There are four main parameters that affect the transfer quality substantially: 1. RPM, 2. RPM ratio of the stamp side roller to the substrate side roller, 3. Gap between the film and substrate, 4. Solvent evaporation time of solution processed r-GO after dropcasting on the stamp surface. Even if r-GO thin films are ready on the stamp surface, transfer never happens without parameter optimization. The microscope glass sheet was selected for the substrate to emphasize the significance of our transfer mechanism. If graphene film is in contact with PDMS and glass, graphene film tends to interact stronger with PDMS as experimentally proven by Matthew Allen et al. (Figure 3.2). With

induced shear stress on the stamp surface cooperating with parameter adjustment, however, transfer takes place regardless of the interfacial characteristics.

Terms used in following sections need to be explained ahead in order for readers to understand experimental setups and results.

- RPM: number of revolutions per minute, used to indicate how fast the rollers rotate.
- Vertical deformation: reduced stamp height by compression during printing process.
- RPM ratio: rotation speed difference in ratio. If it is 1.5, it means the stamp side roller is 1.5 times faster than the other.

3.4.1. Optimization of Dropcasting

Solvent evaporation time during dropcasting film deposition is one of the most important factors that determine the quality of transferred film. Throughout numerous transfer trials with varying solvent evaporation time, it was discovered that shorter evaporation time results in better transfer quality in terms of transferred area and damages on the film as clearly seen in Figure 3.19 and Figure 3.20. In 28 liters vacuum chamber (OV-11, Jeiotech) at vacuum level of -0.096MPa at room temperature (21~22˚C), it takes an hour to vaporize all visible solvent on the stamp surface when 223.2μl of r-GO solvent is drop-cast on stamps. Evaporation time should be longer than one hour at least because r-GO thin film is not formed completely before one hour. Transfer is performed the best at the minimum evaporation time and this is attributed to un-evaporated solvent molecules on the film. Liquid phase molecules have higher mobility so that molecules reorient and inter-diffuse across the contact interface, thus making stronger adhesion between the r-GO thin film and the substrate [68]. To enhance the adhesion between surfaces, contact area has to be maximized and thus surface roughness should be minimized. The surface roughness of the r-GO thin film was examined with evaporation time as a variable (roughness measurement was conducted by AFM non-contact mode). It is observed that roughness becomes bigger as evaporation time increases as shown in Figure 3.21. This is possibly ascribed to remaining solvent molecules that fill nano and micro sized dents.

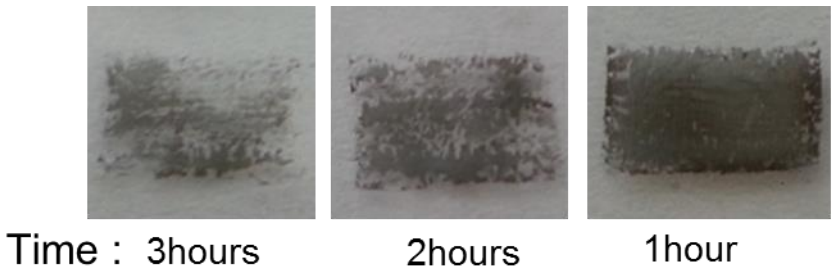

Figure 3.19. **r-GO thin films transferred onto glass substrates with varying solvent evaporation time (with other parameters fixed at RPM ratio: 1.4, vertical deformation: 0.5mm, and RPM: 0.05). Shorter evaporation time results in better transfer.**

Figure 3.20. **Microscopic pictures of r-GO thin films transferred after solvent evaporation time of (a) 3 hours, (b) 2 hours, and (c) 1 hour.**

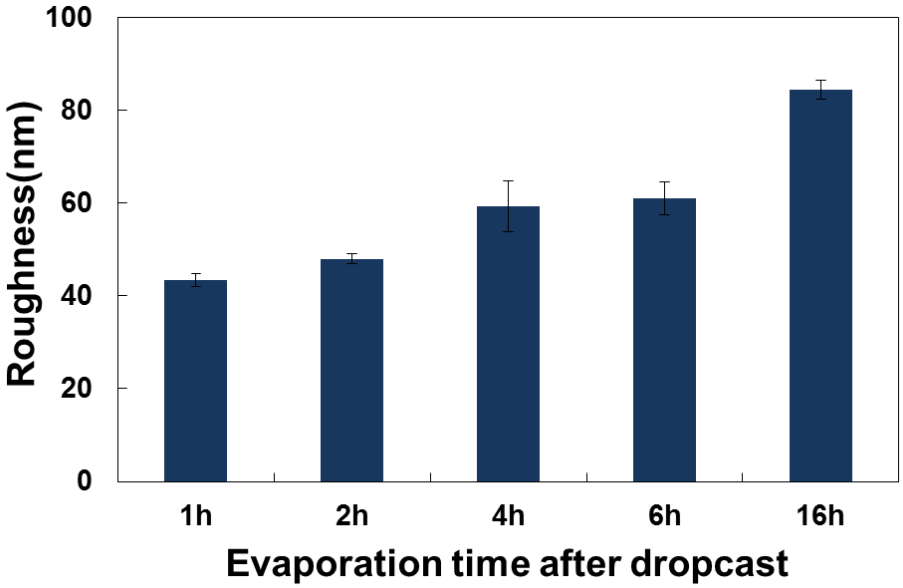

Figure 3.21. **Root mean squared roughness of the r-GO thin film surface according to solvent evaporation time. Roughness is proportional to solvent evaporation time.**

3.4.2. Control of RPM for Two Rolls' Contact Time Variation

RPM is directly related to contact time of the stamp and the substrate. The slower RPM, the longer the r-GO thin film stays in contact with the substrate. It is generally known as a common phenomenon that longer contact time results in stronger adhesion because molecules on the surface rearrange themselves during the contact time to have stronger interaction [68]. In our case, there are un-evaporated solvent molecules on the film surface, thus taking more advantages of stronger adhesion by longer contact time. Experimental results are well matched with the assumption. Transfer experiments were done using different RPMs of the substrate side roller with other parameters fixed at the values that show the best transfer so far(RPM ratio: 1.4, vertical deformation: 0.5mm, evaporation time: 1 hour).

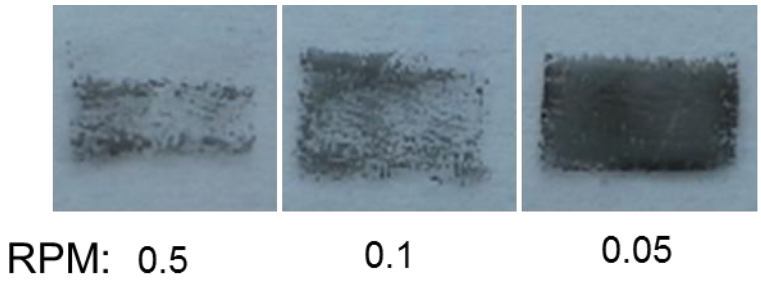

Figure 3.22. r-GO thin films transferred onto glass substrates by different RPMs (with other parameters fixed at RPM ratio: 1.4, vertical deformation: 0.5mm, and evaporation time: 1 hour). Slower RPM gives more contact time during transfer, thus improving transfer.

As shown in Figure 3.22, the transferred area of r-GO thin films is much bigger when RPM is lower. Throughout experiments, it is observed that RPM of 0.05 is giving enough contact time for the film transfer.

3.4.3. Control of Rolls' Gap for Vertical Deformation Variation

Vertical deformation induced on the stamp post during roll-to-roll contact printing provides pressure on the film, ensuring intimate contact. To find the effect of vertical

deformation, transfer experiments were done with different vertical deformation sizes by adjusting the gap between the two rollers. Vertical deformation under 0.2 mm could not make enough pressure in the interface to have sufficient friction to prevent slipping behaviour by exerted shear stress before r-GO thin film is delaminated from the stamp surface. Figure 3.23 informs that vertical deformation from 0.5mm produces adequate pressure in the interface to transfer large area of r-GO thin films. Higher pressure by squeezing the stamp allows r-GO thin film to contact more tightly to the substrate increasing contact area but also vertical direction contraction enlarges the stamp surface in lateral direction which causes cracks in the transferred films [68]. As shown Figure 3.24, vertical deformation of 1mm ends up with more and larger cracks compared to the film transferred with vertical deformation of 0.5mm. Considering experiment data so far, 0.5mm was chosen as vertical deformation value.

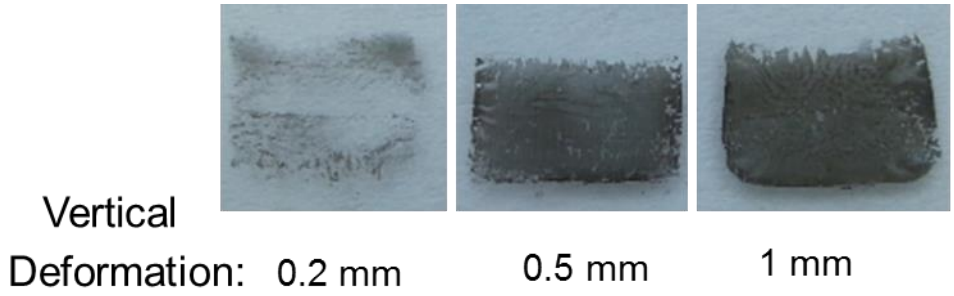

Figure 3.23. r-GO thin films transferred onto glass substrates by vertical deformations of the stamp post. (with other parameters fixed at RPM: 0.05, RPM ratio: 1.4, and evaporation time: 1 hour). Enough vertical pressure has to be induced to have intimate contact between the film and the substrate throughout the transfer.

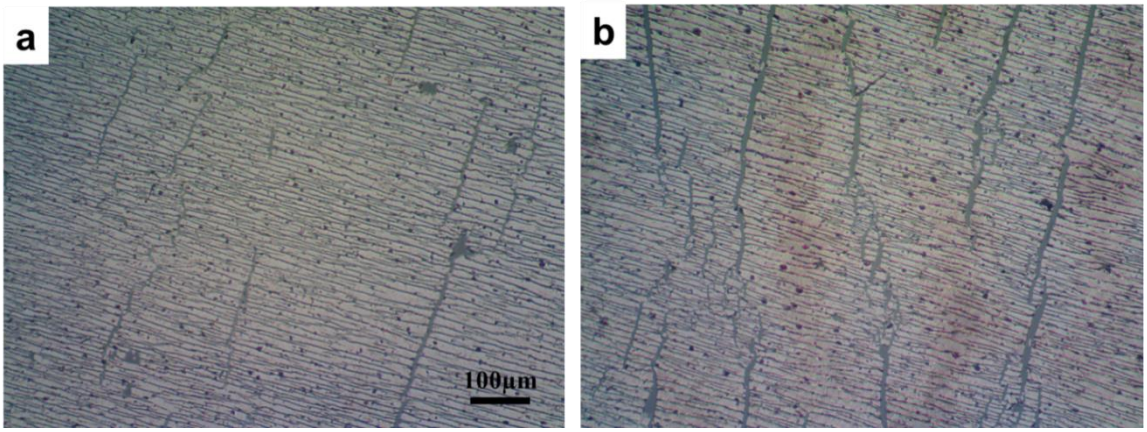

Figure 3.24. Microscopic pictures of transferred r-GO thin film when vertical deformation is (a) 0.5mm and (b) 1mm. Excess pressure caused the stamp to expand in lateral direction creating bigger cracks.

3.4.4. Control of RPM Ratio for Shear Generation

Having different RPMs on the rollers is a way to induce shear stress in a roll-to-roll or roll-to-plate printing system. Our roll-to-roll printing apparatus was design to be able to control two rollers separately. The roller on which the stamp is mounted rotates faster than the substrate side roller, thus making lateral direction displacement on the stamp post as depicted in Figure 3.3. Lateral direction displacement draws shear strain on the stamp post eventually inducing shear stress on the stamp surface.

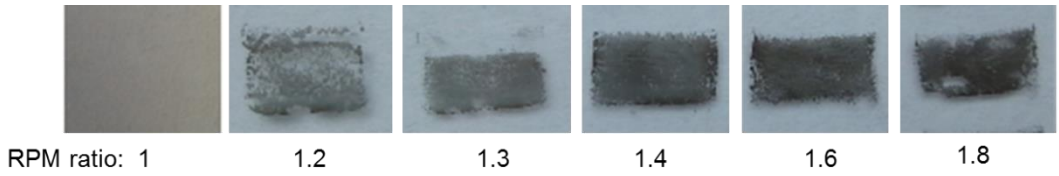

Figure 3.25. r-GO thin films transferred onto glass substrates by different RPM ratios (with other parameters fixed at RPM: 0.05, vertical deformation: 0.5 mm, and evaporation time: 1 hour). The film is not transferred without inducing shear but the film starts being transferred as RPM ratio increases.

Experiment results show that there is a certain point where r-GO thin films start to be transferred to the substrate over whole stamp surface. To compare only the effect of different RPM ratios, other parameters were fixed at the values attained through experiments addressed ahead (evaporation time: 1 hour, RPM of the substrate side

roller: 0.05, vertical deformation: 0.5mm). RPM ratio was raised from 1.2 to 1.8 (films were not transferred at all without having different RPMs) and it seems it obtains enough energy to transfer the films from RPM ratio of 1.4 (Figure 3.25).

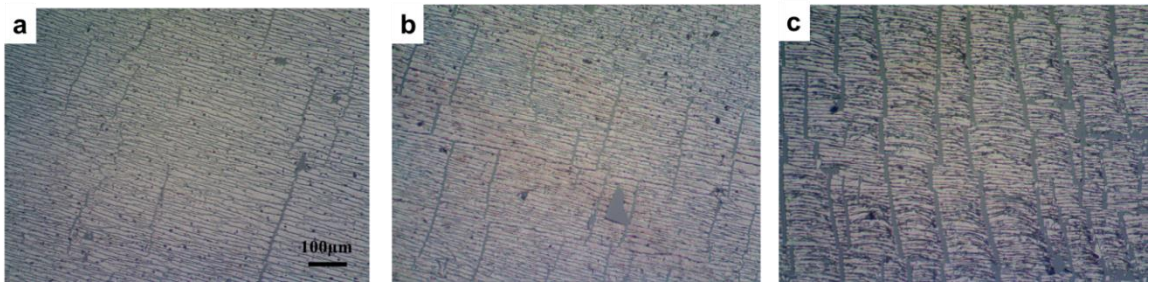

Figure 3.26. Microscopic pictures of r-GO thin films transferred by RPM ratio of (a)1.4, (b)1.6, and (c)1.8. Higher stress induced by higher RPM ratio forms more cracks and wrinkles on the transferred film.

Figure 3.26 shows microscopic pictures of films transferred by different RPM ratios. Though the films were transferred onto the substrate without significant loss of the film, cracks and wrinkles which were found on the film surface increased in size as RPM ratio increases. This is attributed to excessive shear stress exerted by high RPM ratios as explained in the previous section. Because of the damages on the film, the film transferred by RPM ratio of 1.8 has much higher sheet resistance (more than double) than the film transferred by RPM ratio of 1.4 has.

The adjusted parameters so far were also once applied to transferring r-GO thin film onto a flexible and transparent substrate, Polyethylene terephthalate (PET). The result is shown in Figure 3.27. Almost the whole film area was transferred onto a PET substrate but there are more cracks on the film when it is compared with r-GO thin films transferred onto a glass substrate. This is because the interaction that the film has with a glass substrate is different from the interaction with PET. Therefore, the parameters have to be adjusted again for a new material and it has to be done for all other substrates.

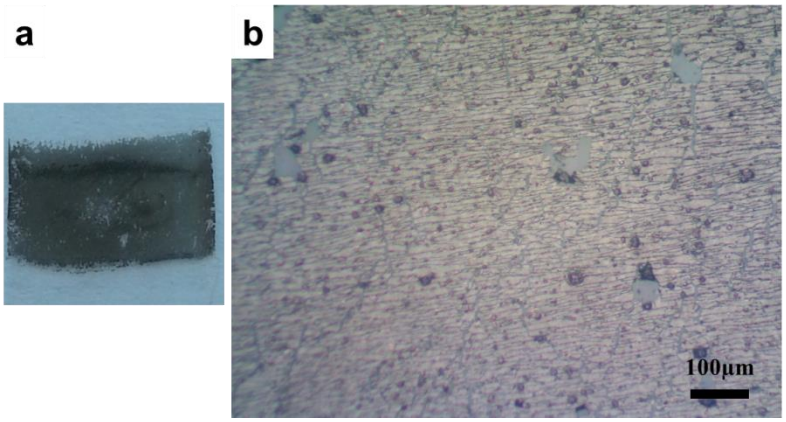

Figure 3.27. Transfer trial onto a flexible polymer substrate: (a) Transferred r-GO onto a PET substrate and (b) the microscopic picture.

The polydopamine coating on the stamp was found to be damaged at the transfer process. r-GO solution was drop-cast on a stamp used once for a transfer. The resulting film on the stamp covered the whole stamp surface but was not evenly deposited as seen in Figure 3.13(c). This means that polydopamine is not evenly covering the stamp after a transfer, implying that some portion of polydopamine is remaining on r-GO thin films after transfer. This is because bonding between polydopamine itself is weaker than its bonding to the stamp and the film [66]. The existence of polydopamine residues on transferred r-GO thin films is verified by ATR-IR spectroscopy in 3.5 Post-Treatment of Transferred r-GO Thin Film.

3.5. Post-Treatment of Transferred r-GO Thin Films

The transferred r-GO thin film as an electrode needs to be improved in terms of the electrical property. There are many factors that degrade electrical conductivity of r-GO thin film by breaking the sp^2 network of graphene such as solvent molecules trapped in r-GO flakes, oxygen groups survived from the reduction process, polydopamine residues, and residues from hydrazine monohydrate. Those impurities should be eliminated to restore the conductivity of graphene. Among many strategies for r-GO optimization, an annealing process after the chemical reduction has been known to be effective [69][70][71][72]. Eda et al.[72] found that the hydrazine reduction of GO followed by a low thermal annealing process at 200˚C can produce r-GO thin films that have better electrical conductivity than r-GO thin films reduced only by thermal annealing

at 550˚C have [73]. This is because each process removes different oxygen functional groups selectively, complementing each other [69].

Annealing process was done for our transferred r-GO thin films with different temperatures. The chemical composition and the sheet resistance were investigated using ATR-IR spectroscopy and a 4-probe sheet resistance measurement system (Keitheley 2400) respectively. The transferred r-GO thin films were put into a vacuum oven of vacuum level -0.096MPa and annealed for 12 hours at 100, 150, 200, and 260˚C.

Figure 3.28 lists the ATR-IR spectra of GO, r-GO and polydopamine films. It can be easily found that the r-GO thin film drop-cast on a glass sheet and the transferred r-GO thin film show different spectra. The only difference between them is presence of polydopamine residues on the transferred r-GO thin film. Since the transferred r-GO thin film was drop-cast on a polydomine modified stamp, there should be residues of polydopamine on it. The transferred r-GO thin film (before annealing process) has three new peaks (844cm^{-1}, 1261cm^{-1} and 1040cm^{-1}) that the r-GO thin film drop-cast on a glass sheet does not have. Considering the ATR-IR spectrum of polydopamine has the same three peaks, it is confirmed that there are polydopamine residues on the transferred r-GO thin films. As annealing temperature increases, the spectra of the transferred films become more similar to that of r-GO thin films without polydopamine residues, meaning decomposition of polydopamine residues.

The annealing process decreased the sheet resistance of the transferred r-GO thin film dramatically. The sheet resistance measurement results are listed in Table 3.1. The decomposition of polydopamine at high temperature should contribute to the resistance decrease as well as evaporation of solvent molecules. The large resistance drop at 100 and 150˚C is ascribed to evaporation of trapped solvent molecules. The further reduction in sheet resistance at 200˚C is possibly due to more rapid evaporation of trapped DMF molecules. Annealing at 260˚C possibly caused the loss of CO and CO_2 from decomposition of labile oxygen functional groups, thus leading to higher conductivity [61].

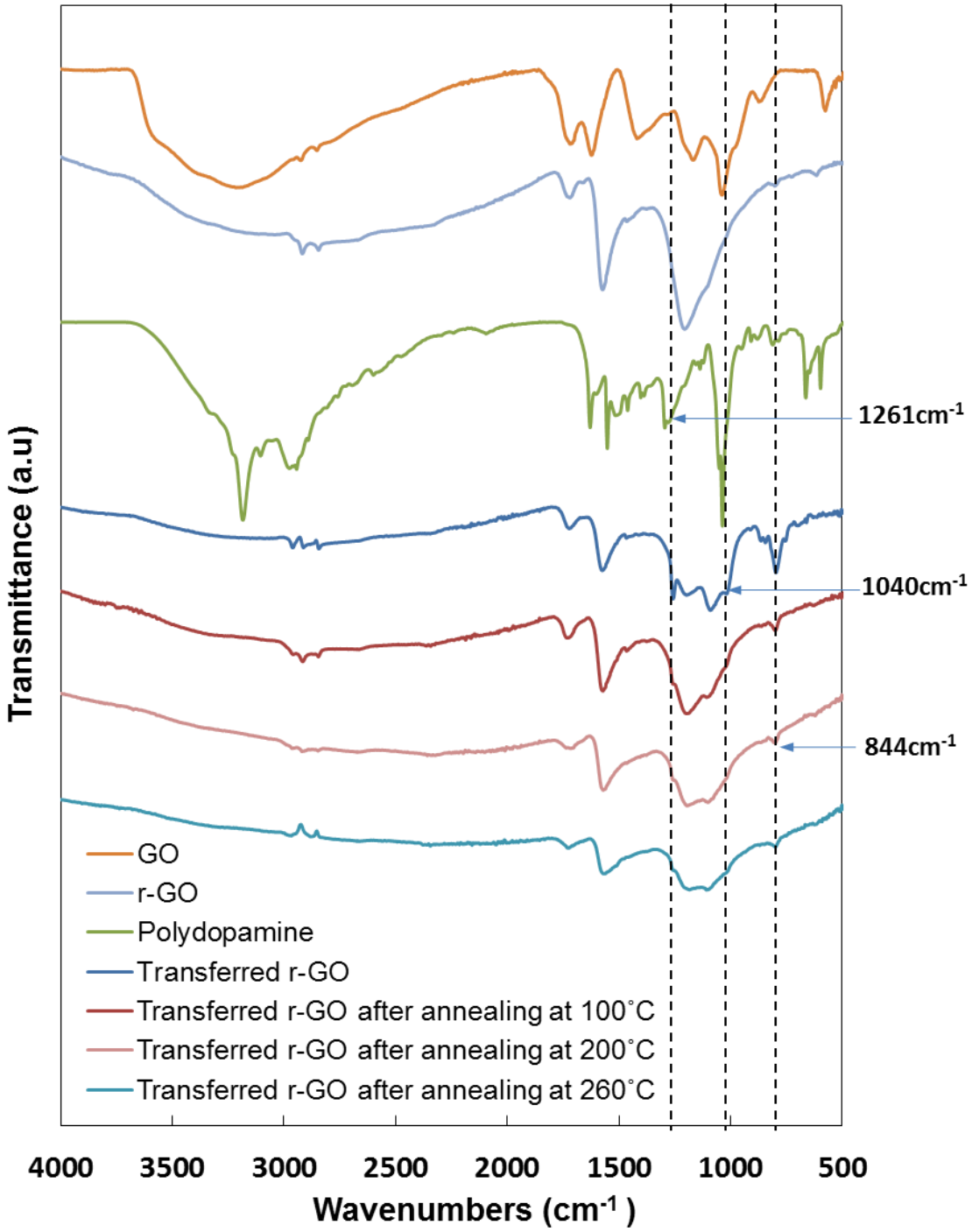

Figure 3.28. **ATR-IR spectra of GO, r-GO, and dopamine films. Polydopamine residues changes the spectrum of transferred r-GO and the spectrum is restored after thermal annealing.**

Table 3.1. Sheet resistance of transferred r-GO thin films before and after annealing at different temperatures.

Temperature(˚C)	Sheet resistance(MΩ/□)
No annealing	38.16
100	16.32
150	2.1
200	0.7
260	0.22

3.6. Demonstration of Transferred Thin Film as Flexible Transparent Electrode

A flexible transparent capacitive touch sensor was fabricated to demonstrated transferred r-GO thin film as flexible transparent electrode. Figure 3.29 (a) shows the device structure. 6 r-GO thin films as touch panels were printed on PET in our roll-to-roll apparatus at a time. This time, only half the amount of r-GO solution used in experiments was used to make the touch panels more transparent. The printed r-GO panels were annealed at 150˚C (PET can be degraded at higher temperature) to improve conductivity. The resulting touch panels have 52% transmittance at 550nm wavelength and sheet resistance of 2.18MΩ/□. The optical transmittance increased 30% while the sheet resistance increased 5.7% by using half the amount of r-GO solution. Printed touch panels were connected to a commercially available capacitive touch sensor breakout board (MPR121, Sparkfun) by enameled wires. The breakout board has its built-in capacitors and one electrode of each capacitor is connected to a touch panel so that the capacitance of the capacitor can be changed by touching the touch panel. The capacitance change signal is converted into voltage output signal by the analog to digital converter in the breakout board and the microprocessor (Arduino Uno) to light up light emitting diodes (LEDs) according to the touch input from the touch panels. Printed touch panels were wrapped on a syringe as seen in Figure 3.29 (b) and LEDs were turned on when fingers were in contact with PET right above the printed touch panels as shown in Figure 3.29 (c).

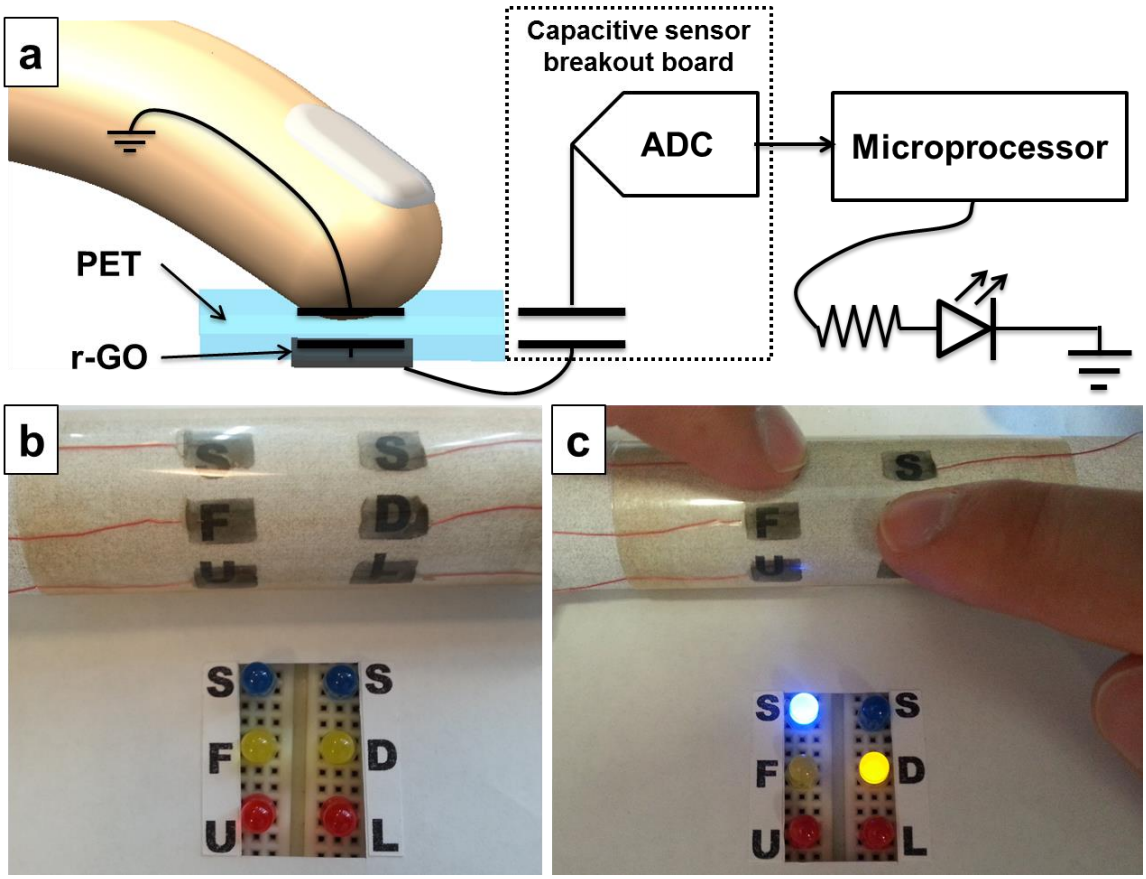

Figure 3.29. (a) Schematic illustration of the capacitive touch sensor with printed r-GO thin film. (b) picture of the flexible transparent capacitive touch sensor. (c) LEDs lightening according to signals from touch input.

3.7. Summary

Shear-induced transfer printing of r-GO thin films has been demonstrated in a roll-to-roll system followed by the introduction of an effective film deposition method. All the processes including r-GO thin film deposition on the stamp, shear-induced transfer, and the film optimization are addressed in detail, and the mechanisms behind the parameter optimization are discussed in this chapter.

Uniform r-GO thin film deposition on the hydrophobic PDMS surface has been enabled by the polydopamine surface modification process. 15 minutes of stamp modification at 60˚C in the dopamine solution (1g/l) has been found to be enough to achieve hydrophilicity required to uniformly deposit r-GO thin films by dropcasting. The

effect of polydopamine modification was observed to be weakened after the stamp had been used for a transfer. This is because some polydopamine also moved onto the r-GO thin film during transfer.

Four parameters in shear-induced roll-to-roll transfer were adjusted through experiments. Solvent evaporation time during the dropcasting process has to be minimized as long as the film is formed on the stamp and there is no visible solvent left on the film. Invisible solvent molecules left on the surface have been known to enhance the adhesion between the r-GO thin film and the substrate. RPM of rollers directly corresponds to contact time of r-GO thin films to the substrate. Contact time is an important factor in contact printing because surface molecules need time to rearrange themselves to maximize the interaction. RPM of the substrate side roller has been adjusted to 0.05 for the best film transfer quality and fast transfer (printing rate: 5mm/min). Vertical deformation is a parameter for giving vertical pressure on the transfer interface. Too much vertical induce deformation in stamp resulting in cracks on the film and too small vertical force does not make tight and intimate contact between the film and the substrate. Vertical deformation of 0.5 mm shows the best transfer results. RPM ratio, the key factor in this transfer method, is to give shear stress on the stamp surface, thus increasing the strain energy release rate until it exceeds the interfacial toughness between the r-GO thin film and the substrate. RPM ratio of 1.4 induced enough shear stress (325.43 kPa) on the stamp surface to trigger delamination over the whole r-GO thin film area, while minimizing excessive energy dissipation onto the film though it was not able to transfer r-GO thin films with no wrinkle and crack. These acquired parameters enabled successful transfer of r-GO thin films onto PET substrates. And these can be reference for the transfer of different materials with different parameters for the future.

The transferred r-GO thin films were remarkably improved in terms of electrical conductivity through an annealing process. The sheet resistance of r-GO decreased more than 170 times after annealing the film at 260˚C for 12 hours in vacuum condition. This is attributed to the evaporation of remained solvent molecules and decomposition of residues from the polydopamine layer on the stamp. The presence of polydopamine

residues on the transferred film was confirmed by ATR-IR spectroscopy, also meaning the polydopamine layer on the stamp is damaged during transfer.

A flexible transparent touch sensor was fabricated with printed r-GO touch panels to demonstrate our printed r-GO thin film as flexible transparent electrode. r-GO thin films were printed on PET using half the amount of r-GO used in other experiments to make the touch panel more transparent. The optical transmittance increased 30% and the sheet resistance increased 5.7% by using half the amount of r-GO. The touch panels were wrapped on a syringe to demonstrate its flexibility and the touch sensing performance was demonstrated by lighting LEDs according to touch signals by fingers.

Chapter 4.

Conclusion and Future Work

4.1. Conclusion

This thesis work has focused on the development of transfer technology that can cooperate with various printing technologies in a roll-to-roll manufacturing system for printed electronics. A novel transfer mechanism, named shear-induced transfer was developed and explored through experiments. A roll-to-roll printing apparatus was designed and fabricated for the thorough investigation on the printing method and demonstrated the transfer of r-GO thin films using the roll-to-roll system. Also, an effective way of r-GO thin film deposition on hydrophobic surface is introduced.

Shear-induced transfer can transfer r-GO thin film onto arbitrary substrates without using chemicals, heat, adhesive, and any expensive conditions. Induced shear stress on the interface between the film and the stamp triggers the delamination of the film. A roll-to-roll apparatus was designed and built to be able to control rollers separately to induce shear stress on the stamp surface. Using the roll-to-roll apparatus, it has been proved that shear-induced transfer can work in a roll-to-roll manufacturing system at a printing rate of 5mm/min. In this thesis, only r-GO as a thin film was chosen for the transfer experiments, but there should be many other thin films that can employ this mechanism though different materials will need different parameter values.

The film deposition process introduced in this thesis also can significantly influence manufacturing systems. PDMS is an attractive material to be used as a stamp in printing systems for its ability to make conformal contact on any substrate and easy patterning method. However, its hydrophobic surface property has been hindering its use in a wide range of film deposition and transfer, transfer printing in particular. Organic

material films had to be formed on another substrate and transfer onto a PDMS stamp to be ready for a transfer because organic materials are mostly processed in aqueous solution that cannot wet the hydrophobic surfaces. The polydopamine modification method enabled direct deposition of solution processed materials on the PDMS stamp. Polydopamine changed the PDMS surface to hydrophilic so that any solution based organic material can form a thin film on the stamp. This made transfer printing simpler since it is now one step direct film deposition on the stamp and one transfer step.

It is expected that technologies introduced in this thesis improve manufacturing systems for printed electronics, giving one good option to roll-to-roll printing system especially where r-GO thin films are necessary. Although r-GO thin films used in this thesis do not have as good electrical properties as pristine graphene has, the unique properties of r-GO can have its applications in different areas. Also, there are doping [74] and alternative synthesis methods [25] already available for solution based r-GO of better electrical properties, and enhancing the electrical properties of solution processed graphene is a matter of time since countless researchers are developing better quality solution processed graphenes.

4.2. Future Work

The work performed in this thesis project suggests several possible improvements recommended to be done in the future.

4.2.1. Transfer to Other Substrates

The transfer experiments of r-GO thin films were mainly done with glass substrates in this project. Though PET substrates were used to demonstrate the transfer onto a flexible polymer substrate, the parameter optimization still needs to be done for the best transfer quality. Likewise, the optimization process has to be rendered for other substrate materials to employ the transfer mechanism to roll-to-roll systems for various printed electronics.

4.2.2. Increasing Printing Speed

The printing rate with our roll-to-roll apparatus for r-GO thin film is now 5mm/min, which is not as fast as other existing roll-to-roll systems. Since printing speed is one of main factors in manufacturing systems, it has to be proved further. To make printing rate higher, printing parameters have be optimized by 4 dimensional optimization process understanding relations between parameters.

4.2.3. Reducing Wrinkles on Transferred r-GO Thin Films

r-GO thin films transferred by shear-induced transfer mechanism have wrinkles on them. The direction of wrinkles is always vertical to the printing direction. This happens because the induced shear force on the stamp also shrinks the stamp surface along the printing direction. Wrinkles can be positively used in that it can give some directional stretchability to the printed electrode when it is printed on flexible material, but there are cases in which wrinkles have negative effects.

To reduce wrinkle generation, the stamp has to be modified. The material for stamp surface should be stiffer than the material for the stamp post. When stamp surface is more rigid than the stamp post is, the deformation induced by mechanical stress tends to be concentrated more on the less rigid stamp post, eventually making less shrinkage on the surface during transfer.

References

[1] M. M. Rodgers, V. M. Pai, and R. S. Conroy, “Recent Advances in Wearable Sensors for Health Monitoring,” *IEEE Sens. J.*, vol. 15, no. 6, pp. 3119–3126, Jun. 2015.

[2] J. Chen and C. T. Liu, “Technology Advances in Flexible Displays and Substrates,” *IEEE Access*, vol. 1, pp. 150–158, 2013.

[3] H. T. Jeong, B. C. Kim, M. J. Higgins, and G. G. Wallace, “Highly stretchable reduced graphene oxide (rGO)/single-walled carbon nanotubes (SWNTs) electrodes for energy storage devices,” *Electrochimica Acta*, vol. 163, pp. 149–160, May 2015.

[4] K. S. Novoselov, A. K. Geim, S. V. Morozov, D. Jiang, Y. Zhang, S. V. Dubonos, I. V. Grigorieva, and A. A. Firsov, “Electric Field Effect in Atomically Thin Carbon Films,” *Science*, vol. 306, no. 5696, pp. 666–669, Oct. 2004.

[5] K. S. Novoselov, A. K. Geim, S. V. Morozov, D. Jiang, M. I. Katsnelson, I. V. Grigorieva, S. V. Dubonos, and A. A. Firsov, “Two-dimensional gas of massless Dirac fermions in graphene,” *Nature*, vol. 438, no. 7065, pp. 197–200, Nov. 2005.

[6] E. V. Castro, K. S. Novoselov, S. V. Morozov, N. M. R. Peres, J. M. B. L. dos Santos, J. Nilsson, F. Guinea, A. K. Geim, and A. H. C. Neto, “Biased Bilayer Graphene: Semiconductor with a Gap Tunable by the Electric Field Effect,” *Phys. Rev. Lett.*, vol. 99, no. 21, p. 216802, Nov. 2007.

[7] S. Pang, Y. Hernandez, X. Feng, and K. Müllen, “Graphene as Transparent Electrode Material for Organic Electronics,” *Adv. Mater.*, vol. 23, no. 25, pp. 2779–2795, Jul. 2011.

[8] A. Fasolino, J. H. Los, and M. I. Katsnelson, “Intrinsic ripples in graphene,” *Nat. Mater.*, vol. 6, no. 11, pp. 858–861, Nov. 2007.

[9] K. Kim, Z. Lee, W. Regan, C. Kisielowski, M. F. Crommie, and A. Zettl, “Grain Boundary Mapping in Polycrystalline Graphene,” *ACS Nano*, vol. 5, no. 3, pp. 2142–2146, Mar. 2011.

[10] D. R. Dreyer, R. S. Ruoff, and C. W. Bielawski, “From Conception to Realization: An Historial Account of Graphene and Some Perspectives for Its Future,” *Angew. Chem. Int. Ed.*, vol. 49, no. 49, pp. 9336–9344, Dec. 2010.

[11] Q. Zheng, Z. Li, J. Yang, and J.-K. Kim, “Graphene oxide-based transparent conductive films,” *Prog. Mater. Sci.*, vol. 64, pp. 200–247, Jul. 2014.

[12] Y. Zhang, J. P. Small, W. V. Pontius, and P. Kim, “Fabrication and electric-field-dependent transport measurements of mesoscopic graphite devices,” *Appl. Phys. Lett.*, vol. 86, no. 7, p. 073104, Feb. 2005.

[13] D. Li, W. Windl, and N. P. Padture, “Toward Site-Specific Stamping of Graphene,” *Adv. Mater.*, vol. 21, no. 12, pp. 1243–1246, Mar. 2009.

[14] X. Liang, Z. Fu, and S. Y. Chou, “Graphene Transistors Fabricated via Transfer-Printing In Device Active-Areas on Large Wafer,” *Nano Lett.*, vol. 7, no. 12, pp. 3840–3844, Dec. 2007.

[15] K. S. Kim, Y. Zhao, H. Jang, S. Y. Lee, J. M. Kim, K. S. Kim, J.-H. Ahn, P. Kim, J.-Y. Choi, and B. H. Hong, “Large-scale pattern growth of graphene films for stretchable transparent electrodes,” *Nature*, vol. 457, no. 7230, pp. 706–710, Feb. 2009.

[16] N. G. Shang, P. Papakonstantinou, M. McMullan, M. Chu, A. Stamboulis, A. Potenza, S. S. Dhesi, and H. Marchetto, “Catalyst-Free Efficient Growth, Orientation and Biosensing Properties of Multilayer Graphene Nanoflake Films with Sharp Edge Planes,” *Adv. Funct. Mater.*, vol. 18, no. 21, pp. 3506–3514, Nov. 2008.

[17] A. Dato, V. Radmilovic, Z. Lee, J. Phillips, and M. Frenklach, “Substrate-free gas-phase synthesis of graphene sheets,” *Nano Lett.*, vol. 8, no. 7, pp. 2012–2016, Jul. 2008.

[18] Q. Yu, J. Lian, S. Siriponglert, H. Li, Y. P. Chen, and S.-S. Pei, “Graphene segregated on Ni surfaces and transferred to insulators,” *Appl. Phys. Lett.*, vol. 93, no. 11, p. 113103, Sep. 2008.

[19] S. Bae, H. Kim, Y. Lee, X. Xu, J.-S. Park, Y. Zheng, J. Balakrishnan, T. Lei, H. Ri Kim, Y. I. Song, Y.-J. Kim, K. S. Kim, B. Özyilmaz, J.-H. Ahn, B. H. Hong, and S. Iijima, “Roll-to-roll production of 30-inch graphene films for transparent electrodes,” *Nat. Nanotechnol.*, vol. 5, no. 8, pp. 574–578, Aug. 2010.

[20] T. Kobayashi, M. Bando, N. Kimura, K. Shimizu, K. Kadono, N. Umezu, K. Miyahara, S. Hayazaki, S. Nagai, Y. Mizuguchi, and others, “Production of a 100-m-long high-quality graphene transparent conductive film by roll-to-roll chemical vapor deposition and transfer process,” *Appl. Phys. Lett.*, vol. 102, no. 2, p. 023112, 2013.

[21] S. J. Kang, B. Kim, K. S. Kim, Y. Zhao, Z. Chen, G. H. Lee, J. Hone, P. Kim, and C. Nuckolls, “Inking Elastomeric Stamps with Micro-Patterned, Single Layer Graphene to Create High-Performance OFETs,” *Adv. Mater.*, vol. 23, no. 31, pp. 3531–3535, Aug. 2011.

[22] D. Li, M. B. Müller, S. Gilje, R. B. Kaner, and G. G. Wallace, “Processable aqueous dispersions of graphene nanosheets,” *Nat. Nanotechnol.*, vol. 3, no. 2, pp. 101–105, Feb. 2008.

[23] S. Wang, P. K. Ang, Z. Wang, A. L. L. Tang, J. T. L. Thong, and K. P. Loh, “High Mobility, Printable, and Solution-Processed Graphene Electronics,” *Nano Lett.*, vol. 10, no. 1, pp. 92–98, Jan. 2010.

[24] H. Liu, L. Zhang, Y. Guo, C. Cheng, L. Yang, L. Jiang, G. Yu, W. Hu, Y. Liu, and D. Zhu, “Reduction of graphene oxide to highly conductive graphene by Lawesson’s reagent and its electrical applications,” *J. Mater. Chem. C*, vol. 1, no. 18, p. 3104, 2013.

[25] K. Parvez, R. Li, S. R. Puniredd, Y. Hernandez, F. Hinkel, S. Wang, X. Feng, and K. Müllen, “Electrochemically Exfoliated Graphene as Solution-Processable, Highly Conductive Electrodes for Organic Electronics,” *ACS Nano*, vol. 7, no. 4, pp. 3598–3606, Apr. 2013.

[26] R. Garg, N. K. Dutta, and N. R. Choudhury, “Work Function Engineering of Graphene,” *Nanomaterials*, vol. 4, no. 2, pp. 267–300, Apr. 2014.

[27] W. S. Hummers and R. E. Offeman, “Preparation of Graphitic Oxide,” *J. Am. Chem. Soc.*, vol. 80, no. 6, pp. 1339–1339, Mar. 1958.

[28] S. Park and R. S. Ruoff, “Chemical methods for the production of graphenes,” *Nat. Nanotechnol.*, vol. 4, no. 4, pp. 217–224, Apr. 2009.

[29] G. Wang, J. Yang, J. Park, X. Gou, B. Wang, H. Liu, and J. Yao, “Facile Synthesis and Characterization of Graphene Nanosheets,” *J. Phys. Chem. C*, vol. 112, no. 22, pp. 8192–8195, Jun. 2008.

[30] U. Hofmann and A. Frenzel, “Die Reduktion von Graphitoxyd mit Schwefelwasserstoff,” *Kolloid-Z.*, vol. 68, no. 2, pp. 149–151, Aug. 1934.

[31] R. Muszynski, B. Seger, and P. V. Kamat, “Decorating Graphene Sheets with Gold Nanoparticles,” *J. Phys. Chem. C*, vol. 112, no. 14, pp. 5263–5266, Apr. 2008.

[32] G. K. Ramesha and S. Sampath, “Electrochemical Reduction of Oriented Graphene Oxide Films: An in Situ Raman Spectroelectrochemical Study,” *J. Phys. Chem. C*, vol. 113, no. 19, pp. 7985–7989, May 2009.

[33] X. Wang, L. Zhi, and K. Müllen, “Transparent, conductive graphene electrodes for dye-sensitized solar cells,” *Nano Lett.*, vol. 8, no. 1, pp. 323–327, Jan. 2008.

[34] E. B. Secor, S. Lim, H. Zhang, C. D. Frisbie, L. F. Francis, and M. C. Hersam, “Gravure Printing of Graphene for Large-area Flexible Electronics,” *Adv. Mater.*, vol. 26, no. 26, pp. 4533–4538, Jul. 2014.

[35] J. Baker, D. Deganello, D. T. Gethin, and T. M. Watson, “Flexographic printing of graphene nanoplatelet ink to replace platinum as counter electrode catalyst in flexible dye sensitised solar cell,” *Mater. Res. Innov.*, vol. 18, no. 2, pp. 86–90, Feb. 2014.

[36] E. B. Secor, P. L. Prabhumirashi, K. Puntambekar, M. L. Geier, and M. C. Hersam, “Inkjet Printing of High Conductivity, Flexible Graphene Patterns,” *J. Phys. Chem. Lett.*, vol. 4, no. 8, pp. 1347–1351, Apr. 2013.

[37] W. J. Hyun, E. B. Secor, M. C. Hersam, C. D. Frisbie, and L. F. Francis, “High-Resolution Patterning of Graphene by Screen Printing with a Silicon Stencil for Highly Flexible Printed Electronics,” *Adv. Mater.*, vol. 27, no. 1, pp. 109–115, Jan. 2015.

[38] Z. Yin, S. Sun, T. Salim, S. Wu, X. Huang, Q. He, Y. M. Lam, and H. Zhang, “Organic Photovoltaic Devices Using Highly Flexible Reduced Graphene Oxide Films as Transparent Electrodes,” *ACS Nano*, vol. 4, no. 9, pp. 5263–5268, Sep. 2010.

[39] F. Schedin, A. K. Geim, S. V. Morozov, E. W. Hill, P. Blake, M. I. Katsnelson, and K. S. Novoselov, “Detection of individual gas molecules adsorbed on graphene,” *Nat. Mater.*, vol. 6, no. 9, pp. 652–655, Sep. 2007.

[40] J. D. Fowler, M. J. Allen, V. C. Tung, Y. Yang, R. B. Kaner, and B. H. Weiller, “Practical chemical sensors from chemically derived graphene,” *ACS Nano*, vol. 3, no. 2, pp. 301–306, Feb. 2009.

[41] J. T. Robinson, F. K. Perkins, E. S. Snow, Z. Wei, and P. E. Sheehan, “Reduced graphene oxide molecular sensors,” *Nano Lett.*, vol. 8, no. 10, pp. 3137–3140, Oct. 2008.

[42] M. J. Allen, V. C. Tung, and R. B. Kaner, “Honeycomb Carbon: A Review of Graphene,” *Chem. Rev.*, vol. 110, no. 1, pp. 132–145, Jan. 2010.

[43] H. J. Yoon, D. H. Jun, J. H. Yang, Z. Zhou, S. S. Yang, and M. M.-C. Cheng, “Carbon dioxide gas sensor using a graphene sheet,” *Sens. Actuators B Chem.*, vol. 157, no. 1, pp. 310–313, Sep. 2011.

[44] R. Kazemzadeh, K. Andersen, L. Motha, and W. S. Kim, “Highly Sensitive Pressure Sensor Array With Photothermally Reduced Graphene Oxide,” *IEEE Electron Device Lett.*, vol. 36, no. 2, pp. 180–182, Feb. 2015.

[45] N. Kim, S. Kee, S. H. Lee, B. H. Lee, Y. H. Kahng, Y.-R. Jo, B.-J. Kim, and K. Lee, “Highly Conductive PEDOT:PSS Nanofibrils Induced by Solution-Processed Crystallization,” *Adv. Mater.*, vol. 26, no. 14, pp. 2268–2272, Apr. 2014.

[46] P. Peng, A. Hu, H. Huang, A. P. Gerlich, B. Zhao, and Y. N. Zhou, “Room-temperature pressureless bonding with silver nanowire paste: towards organic electronic and heat-sensitive functional devices packaging,” *J. Mater. Chem.*, vol. 22, no. 26, pp. 12997–13001, Jun. 2012.

[47] F. C. Krebs, J. Fyenbo, and M. Jørgensen, “Product integration of compact roll-to-roll processed polymer solar cell modules: methods and manufacture using flexographic printing, slot-die coating and rotary screen printing,” *J. Mater. Chem.*, vol. 20, no. 41, pp. 8994–9001, Oct. 2010.

[48] J. Kim, K. Wubs, B.-S. Bae, and W. Soo Kim, “Direct stamping of silver nanoparticles toward residue-free thick electrode,” *Sci. Technol. Adv. Mater.*, vol. 13, no. 3, p. 035004, Jun. 2012.

[49] Y. Zhu, S. Murali, W. Cai, X. Li, J. W. Suk, J. R. Potts, and R. S. Ruoff, “Graphene and Graphene Oxide: Synthesis, Properties, and Applications,” *Adv. Mater.*, vol. 22, no. 35, pp. 3906–3924, Sep. 2010.

[50] M. J. Allen, V. C. Tung, L. Gomez, Z. Xu, L.-M. Chen, K. S. Nelson, C. Zhou, R. B. Kaner, and Y. Yang, “Soft Transfer Printing of Chemically Converted Graphene,” *Adv. Mater.*, vol. 21, no. 20, pp. 2098–2102, May 2009.

[51] A. L. Briseno, M. Roberts, M.-M. Ling, H. Moon, E. J. Nemanick, and Z. Bao, “Patterning Organic Semiconductors Using ‘Dry’ Poly(dimethylsiloxane) Elastomeric Stamps for Thin Film Transistors,” *J. Am. Chem. Soc.*, vol. 128, no. 12, pp. 3880–3881, Mar. 2006.

[52] K. Glasmästar, J. Gold, A.-S. Andersson, D. S. Sutherland, and B. Kasemo, “Silicone Transfer during Microcontact Printing,” *Langmuir*, vol. 19, no. 13, pp. 5475–5483, Jun. 2003.

[53] “Wiley: Failure of Materials in Mechanical Design: Analysis, Prediction, Prevention, 2nd Edition - Jack A. Collins.” [Online]. Available: http://ca.wiley.com/WileyCDA/WileyTitle/productCd-0471558915.html. [Accessed: 13-Jun-2015].

[54] A. A. Griffith, “The Phenomena of Rupture and Flow in Solids,” *Philos. Trans. R. Soc. Lond. Math. Phys. Eng. Sci.*, vol. 221, no. 582–593, pp. 163–198, Jan. 1921.

[55] A. A. Volinsky, N. R. Moody, and W. W. Gerberich, “Interfacial toughness measurements for thin films on substrates,” *Acta Mater.*, vol. 50, no. 3, pp. 441–466, 2002.

[56] M. L. Jokl, V. Vitek, and C. J. McMahon Jr, “A microscopic theory of brittle fracture in deformable solids: A relation between ideal work to fracture and plastic work,” *Acta Metall.*, vol. 28, no. 11, pp. 1479–1488, Nov. 1980.

[57] R. S. Rivlin and A. G. Thomas, “Rupture of rubber. I. Characteristic energy for tearing,” *J. Polym. Sci.*, vol. 10, no. 3, pp. 291–318, Mar. 1953.

[58] G. C. Sih and B. Macdonald, “Fracture mechanics applied to engineering problems-strain energy density fracture criterion,” *Eng. Fract. Mech.*, vol. 6, no. 2, pp. 361–386, Sep. 1974.

[59] D. P. ROOKE, D. J. Cartwright, Great Britain, Ministry of Defence, and Procurement Executive, *Compendium of stress intensity factors*. London: H.M.S.O., 1976.

[60] S. Park, Y. Hu, J. O. Hwang, E.-S. Lee, L. B. Casabianca, W. Cai, J. R. Potts, H.-W. Ha, S. Chen, J. Oh, S. O. Kim, Y.-H. Kim, Y. Ishii, and R. S. Ruoff, “Chemical structures of hydrazine-treated graphene oxide and generation of aromatic nitrogen doping,” *Nat. Commun.*, vol. 3, p. 638, Jan. 2012.

[61] S. Park, J. An, I. Jung, R. D. Piner, S. J. An, X. Li, A. Velamakanni, and R. S. Ruoff, “Colloidal Suspensions of Highly Reduced Graphene Oxide in a Wide Variety of Organic Solvents,” *Nano Lett.*, vol. 9, no. 4, pp. 1593–1597, Apr. 2009.

[62] J. Zhang, H. Yang, G. Shen, P. Cheng, J. Zhang, and S. Guo, “Reduction of graphene oxide via L -ascorbic acid,” *Chem Commun*, vol. 46, no. 7, pp. 1112–1114, 2010.

[63] S. Park, K.-S. Lee, G. Bozoklu, W. Cai, S. T. Nguyen, and R. S. Ruoff, “Graphene Oxide Papers Modified by Divalent Ions—Enhancing Mechanical Properties via Chemical Cross-Linking,” *ACS Nano*, vol. 2, no. 3, pp. 572–578, Mar. 2008.

[64] H. Lee, S. M. Dellatore, W. M. Miller, and P. B. Messersmith, “Mussel-Inspired Surface Chemistry for Multifunctional Coatings,” *Science*, vol. 318, no. 5849, pp. 426–430, Oct. 2007.

[65] J. Jiang, L. Zhu, L. Zhu, B. Zhu, and Y. Xu, “Surface Characteristics of a Self-Polymerized Dopamine Coating Deposited on Hydrophobic Polymer Films,” *Langmuir*, vol. 27, no. 23, pp. 14180–14187, Dec. 2011.

[66] F. K. Yang and B. Zhao, “Adhesion properties of self-polymerized dopamine thin film,” *Open Surf. Sci. J.*, vol. 3, no. 2, pp. 115–119, 2011.

[67] K.-Y. Ju, Y. Lee, S. Lee, S. B. Park, and J.-K. Lee, “Bioinspired Polymerization of Dopamine to Generate Melanin-Like Nanoparticles Having an Excellent Free-Radical-Scavenging Property,” *Biomacromolecules*, vol. 12, no. 3, pp. 625–632, Mar. 2011.

[68] Y. L. Chen, C. A. Helm, and J. N. Israelachvili, “Molecular mechanisms associated with adhesion and contact angle hysteresis of monolayer surfaces,” *J. Phys. Chem.*, vol. 95, no. 26, pp. 10736–10747, Dec. 1991.

[69] W. Gao, L. B. Alemany, L. Ci, and P. M. Ajayan, “New insights into the structure and reduction of graphite oxide,” *Nat. Chem.*, vol. 1, no. 5, pp. 403–408, Aug. 2009.

[70] H. Chen, M. B. Müller, K. J. Gilmore, G. G. Wallace, and D. Li, “Mechanically Strong, Electrically Conductive, and Biocompatible Graphene Paper,” *Adv. Mater.*, vol. 20, no. 18, pp. 3557–3561, Sep. 2008.

[71] Y. Si and E. T. Samulski, “Synthesis of water soluble graphene,” *Nano Lett.*, vol. 8, no. 6, pp. 1679–1682, Jun. 2008.

[72] G. Eda, G. Fanchini, and M. Chhowalla, “Large-area ultrathin films of reduced graphene oxide as a transparent and flexible electronic material,” *Nat. Nanotechnol.*, vol. 3, no. 5, pp. 270–274, May 2008.

[73] S. Pei and H.-M. Cheng, “The reduction of graphene oxide,” *Carbon*, vol. 50, no. 9, pp. 3210–3228, Aug. 2012.

[74] G. Eda, Y.-Y. Lin, S. Miller, C.-W. Chen, W.-F. Su, and M. Chhowalla, “Transparent and conducting electrodes for organic electronics from reduced graphene oxide,” *Appl. Phys. Lett.*, vol. 92, no. 23, p. 233305, Jun. 2008.